

How to Bend the Uranyl Cation via Crystal Engineering

Korey P. Carter[§], Mark Kalaj[§], Andrew Kerridge[†], J. August Ridenour[§], and Christopher L. Cahill^{*§}

[§] Department of Chemistry, The George Washington University, 800 22nd Street, NW, Washington, D.C. 20052, United States

[†] Department of Chemistry, Lancaster University, Bailrigg, Lancaster LA1 4YB, United Kingdom

E-mail: cahill@gwu.edu

Supporting Info Section

I. Synthesis Procedures for Complexes 1-9

II. Low Temperature (100K) and Room Temperature (293K) XRD Data for Complexes 1-3

III. Additional Single Crystal XRD Data for Complexes 4-12

IV. Additional Figures

V. Additional DFT and QTAIM Data

VI. Vibrational and Luminescence Spectroscopy Data

VII. Powder X-ray Diffraction Data

VIII. Thermal Ellipsoid Plots

IX. Tables of Bond Distances and Bond Angles

X. Bond Valence Summations

XI. References

I. Synthesis Procedures for Complexes 1-9

Materials and Methods

Caution: Whereas the uranium oxyacetate dihydrate $[\text{UO}_2(\text{CH}_3\text{COO})_2] \cdot 2\text{H}_2\text{O}$ and uranyl nitrate hexahydrate $[\text{UO}_2(\text{NO}_3)_2] \cdot 6\text{H}_2\text{O}$ used in this study contained depleted U, standard precautions for handling radioactive and toxic substances should be followed.

All organic materials, benzoic acid (Sigma Aldrich, $\geq 99.5\%$), 2,4,6-trifluorobenzoic acid (246triFBA) (Alfa Aesar, 98%), 2,4,6-trichlorobenzoic acid (246triClBA) (Sigma Aldrich, 97%), 2,4,6-tribromobenzoic acid (246triBrBA) (Sigma Aldrich, 96%), and 1,10-phenanthroline (Alfa Aesar, 99%), were purchased and used as received.

Synthesis of UO_2 -triFBA-Phen complexes $[\text{UO}_2(\text{C}_{12}\text{H}_8\text{N}_2)_2(\text{C}_7\text{H}_2\text{F}_3\text{O}_2)_2] \cdot (\text{C}_{12}\text{H}_8\text{N}_2)$ (**1**) and $[\text{UO}_2(\text{OH})(\text{C}_{12}\text{H}_8\text{N}_2)(\text{C}_7\text{H}_2\text{F}_3\text{O}_2)]_2$ (**4**)

Complexes **1** and **4** co-formed from a reaction combining $\text{UO}_2(\text{CH}_3\text{COO})_2 \cdot 2\text{H}_2\text{O}$ (0.053 g, 0.125 mmol), 2,4,6-trifluorobenzoic acid (0.034 g, 0.25 mmol), 1,10-phenanthroline (0.077 g, 0.4375 mmol), and distilled water (1.5 g, 83.3 mmol) in a Parr autoclave. Reaction pH was adjusted to approximately 2.3 via dropwise addition of 1M HCl and then the reaction vessel was heated statically at 90 °C for 72 hours. The sample was allowed to cool to room temperature and then the Parr autoclave was opened after approximately sixteen hours. Two sets of yellow rectangular plate crystals were obtained from the bulk product after decanting the supernatant liquor, washing three times with distilled water and ethanol, and air-drying at room temperature overnight. These crystals could be hand separated based on crystal color and luminescence under a UV lamp (Figure S1), with crystals of the ‘bent’ complex (**1**) displaying brighter luminescence. This is of particular importance for these two complexes as single crystals of **1** are rare in

the bulk product with no more than ten crystals in any sample (out of approximately 250 single crystals in a single dish). Complex **4** can be isolated as pure phase (confirmed via PXRD, Figure S23) by decreasing the amount of 1,10-phenanthroline used in the reaction and increasing the oven temperature to 150 °C.

Synthesis of UO₂-triCIBA-Phen complexes [UO₂(C₁₂H₈N₂)₂(C₇H₂Cl₃O₂)₂]•2H₂O (**2**) and [UO₂(C₁₂H₈N₂)(C₇H₂Cl₃O₂)₂] (**5**)

Complexes **2** and **5** co-formed from a reaction combining UO₂(CH₃COO)₂•2H₂O (0.053 g, 0.125 mmol), 2,4,6-trichlorobenzoic acid (0.045 g, 0.25 mmol), 1,10-phenanthroline (0.044 g, 0.25 mmol), and distilled water (1.5 g, 83.3 mmol) in a Parr autoclave. Reaction pH was unadjusted from approximately 3.4 and the reaction vessel was heated statically at 150 °C for 72 hours. Similar to complexes **1** and **4**, two sets of yellow rectangular plate crystals were obtained from the bulk product. For **2** and **5**, crystals of the ‘bent’ complex (**2**) were found to luminesce under UV light, whereas for the ‘non-bent’ complex (**5**), crystals displayed no emission (Figure S1). Single crystals of the two phases can be found in approximately equal amounts using the protocol outlined above, and complex **2** was found to be the major phase when oven temperature and reaction time were increased. We were unable to isolate **2** as a pure bulk phase in any reaction despite several dozen attempts, whereas complex **5** can be isolated as pure phase (confirmed via PXRD, Figure S24) by using the same conditions and changing the uranyl starting salt to uranyl nitrate hexahydrate ([UO₂(NO₃)₂]•6H₂O).

Synthesis of UO₂-triBrBA-Phen complexes [UO₂(C₁₂H₈N₂)₂(C₇H₂Br₃O₂)₂] (**3**), [UO₂(OH)(C₁₂H₈N₂)(C₇H₂Br₃O₂)₂] (**6**), and [UO₂(C₁₂H₈N₂)(C₇H₂Br₃O₂)₂] (**7**)

Complexes **3** and **6** co-formed from a reaction combining UO₂(CH₃COO)₂•2H₂O (0.053 g, 0.125 mmol), 2,4,6-tribromobenzoic acid (0.072 g, 0.25 mmol), 1,10-

phenanthroline (0.066 g, 0.375 mmol), and distilled water (1.5 g, 83.3 mmol) in a Parr autoclave. Reaction pH was unadjusted from approximately 3.6 and the reaction vessel was heated statically at 150 °C for 72 hours. Similar to the ‘bent’ and ‘non-bent’ 246triFBA and 246triClBA complexes (**1**, **2**, **4**, and **5**), two sets of yellow rectangular plate crystals were obtained from the bulk product. For **3** and **6**, the crystals of both phases were very similar in size, yet differed substantially in emission upon UV excitation. Crystals of the ‘bent’ complex (**3**) were found to be very luminescent under UV light, whereas for the ‘non-bent’ complex (**6**), crystals displayed a complete lack of emission (Figure S1). These differences in luminescence made isolation of single crystals straightforward even though the ratio of ‘bent’ to ‘non-bent’ complexes was approximately 1:3 across the range of conditions used in this study. Attempts to isolate complex **6** as a pure phase were unsuccessful as adjusting reaction conditions also yielded a third UO₂-triBrBA-Phen complex (**7**), along with a uranyl-phen dimer (complex **8**) (Figures S6 and S7). Subsequent experiments found that complex **7** can be isolated as pure phase (confirmed via PXRD, Figure S26) changing the uranyl starting salt to uranyl nitrate hexahydrate ([UO₂(NO₃)₂]•6H₂O) and decreasing the oven temperature to 120 °C.

Synthesis of non-bent UO₂-BA-Phen complexes
[(UO₂)₂(OH)(O)(C₁₂H₈N₂)(CH₃COO)(H₂O)]₂•2H₂O (**8**) and [UO₂(C₁₂H₈N₂)(C₇H₅O₂)₂]
(**9**)

Complexes **8** and **9** were synthesized by repeating the reaction conditions described above, which yielded complexes **1-3** with benzoic acid (0.024 g, 0.25 mmol) replacing the 2,4,6-trihalobenzoic acid ligand in each reaction mixture. Complex **8** has been characterized previously by our group,¹ yet was synthesized here via a new reaction pathway as these crystals were isolated from the BA reaction using complex **1** conditions.

Replacing 246triCIBA and 246triBrBA with benzoic acid in the reaction mixtures that yielded complexes **2** and **3** both yielded complex **9**. For both **8** and **9**, we were unable to isolate pure bulk phases despite multiple reactions where conditions were systematically adjusted.

II. Low Temperature (100K) and Room Temperature (293K) XRD Data for Complexes 1-3

Table S1 Low temperature (100 K) Crystallographic Data for Complexes 1-3

	1	2	3
chem formula	C ₅₀ H ₂₈ F ₆ N ₆ O ₆ U	C ₃₈ H ₂₄ Cl ₆ N ₄ O ₈ U	C ₃₈ H ₂₀ Br ₆ N ₄ O ₆ U
formula weight	1160.81	1115.34	1346.07
crystal system	triclinic	monoclinic	monoclinic
space group	<i>P</i> -1	<i>P</i> 2 ₁ / <i>n</i>	<i>P</i> 2 ₁ / <i>c</i>
<i>a</i> (Å)	8.5926(13)	9.1607(6)	9.0076(13)
<i>b</i> (Å)	9.6308(14)	20.6520(14)	21.687(3)
<i>c</i> (Å)	25.363(4)	19.8941(13)	19.754(3)
α (deg)	82.011(2)	90	90
β (deg)	87.714(4)	94.250(9)	94.342(2)
γ (deg)	86.441(3)	90	90
<i>V</i> (Å ³)	2073.5(5)	3753.4(4)	3847.8(10)
<i>Z</i>	2	4	4
<i>T</i> (K)	100(2)	100(2)	100(2)
λ (Mo K α)	0.71073	0.71073	0.71073
<i>D</i> _{calc} (g cm ⁻³)	1.859	1.974	2.324
μ (mm ⁻¹)	4.004	4.813	10.502
<i>R</i> _{int}	0.0583	0.0854	0.0775
<i>R</i> ₁ [<i>I</i> >2 σ (<i>I</i>)]	0.0331	0.0375	0.0370
w <i>R</i> ₂ [<i>I</i> >2 σ (<i>I</i>)]	0.0748	0.0820	0.0706

Table S2 Room temperature (293 K) Crystallographic Data for Complexes **1-3**

	1 (RT)	2 (RT)	3 (RT)
chem formula	C ₅₀ H ₂₈ F ₆ N ₆ O ₆ U	C ₃₈ H ₂₄ Cl ₆ N ₄ O ₈ U	C ₃₈ H ₂₀ Br ₆ N ₄ O ₆ U
formula weight	1160.81	1115.34	1346.07
crystal system	triclinic	monoclinic	monoclinic
space group	<i>P</i> -1	<i>P</i> 2 ₁ / <i>n</i>	<i>P</i> 2 ₁ / <i>c</i>
<i>a</i> (Å)	8.7625(3)	9.2741(6)	9.110(3)
<i>b</i> (Å)	9.6750(3)	20.8287(14)	21.813(7)
<i>c</i> (Å)	25.4898(9)	20.1166(13)	19.925(7)
α (deg)	81.958(10)	90	90
β (deg)	87.862(11)	93.720(8)	93.485(6)
γ (deg)	86.194(11)	90	90
<i>V</i> (Å ³)	2134.12(14)	3877.7(4)	3952.0(2)
<i>Z</i>	2	4	4
<i>T</i> (K)	293(2)	293(2)	293(2)
λ (Mo K α)	0.71073	0.71073	0.71073
<i>D</i> _{calc} (g cm ⁻³)	1.806	1.910	2.262
μ (mm ⁻¹)	3.891	4.658	10.225
<i>R</i> _{int}	0.0348	0.0824	0.0570
<i>R</i> ₁ [<i>I</i> >2 σ (<i>I</i>)]	0.0332	0.0402	0.0343
w <i>R</i> ₂ [<i>I</i> >2 σ (<i>I</i>)]	0.0809	0.0855	0.0684

III. Additional Single Crystal XRD Data for Complexes 4-12

Table S3 Crystallographic Data for Complexes 4-12

	4	5	6
chem formula	C ₃₈ H ₂₂ F ₆ N ₄ O ₁₀ U ₂	C ₂₆ H ₁₂ Cl ₆ N ₂ O ₆ U	C ₃₈ H ₂₂ Br ₆ N ₄ O ₁₀ U ₂
formula weight	1284.65	899.11	1650.11
crystal system	triclinic	monoclinic	monoclinic
space group	<i>P</i> -1	<i>P</i> 2 ₁ / <i>n</i>	<i>P</i> 2 ₁ / <i>c</i>
<i>a</i> (Å)	8.6736(17)	8.116(5)	9.1587(3)
<i>b</i> (Å)	9.0364(17)	18.693(11)	21.9335(8)
<i>c</i> (Å)	12.821(3)	19.453(12)	11.5478(4)
α (deg)	106.273(6)	90	90
β (deg)	95.888(3)	98.372(16)	109.030(7)
γ (deg)	99.638(4)	90	90
<i>V</i> (Å ³)	939.1(3)	2920.0(3)	2192.97(16)
<i>Z</i>	1	4	2
<i>T</i> (K)	293(2)	293(2)	293(2)
λ (Mo K α)	0.71073	0.71073	0.71073
<i>D</i> _{calc} (g cm ⁻³)	2.272	2.046	2.499
μ (mm ⁻¹)	8.707	6.153	12.901
<i>R</i> _{int}	0.0342	0.0789	0.0409
<i>R</i> 1 [<i>I</i> >2 σ (<i>I</i>)]	0.0252	0.0424	0.0299
<i>wR</i> 2 [<i>I</i> >2 σ (<i>I</i>)]	0.0529	0.0826	0.0668
	7	8	9
chem formula	C ₂₆ H ₁₂ Br ₆ N ₂ O ₆ U	C ₂₈ H ₃₄ N ₄ O ₂₂ U ₄	C ₂₆ H ₁₈ N ₂ O ₆ U
formula weight	1165.87	1730.71	692.45
crystal system	monoclinic	triclinic	monoclinic
space group	<i>P</i> 2 ₁ / <i>n</i>	<i>P</i> -1	<i>P</i> 2 ₁ / <i>c</i>
<i>a</i> (Å)	16.9062(6)	8.135(3)	9.1706(10)
<i>b</i> (Å)	18.5214(7)	9.685(3)	34.493(4)
<i>c</i> (Å)	20.0739(7)	13.002(4)	7.0488(8)
α (deg)	90	87.858(6)	90
β (deg)	97.772(4)	84.656(5)	90.871(3)
γ (deg)	90	70.824(4)	90
<i>V</i> (Å ³)	6227.9(4)	963.4(6)	2229.4(4)
<i>Z</i>	8	1	4
<i>T</i> (K)	293(2)	100(2)	100(2)

λ (Mo K α)	0.71073	0.71073	0.71073
D_{calc} (g cm $^{-3}$)	2.487	2.983	2.063
μ (mm $^{-1}$)	12.953	16.850	7.328
R_{int}	0.0733	0.0425	0.0256
R1 [$I > 2\sigma(I)$]	0.0422	0.0277	0.0219
wR2 [$I > 2\sigma(I)$]	0.0879	0.0547	0.0437
	10	11	12
chem formula	C ₂₄ H ₁₂ Cl ₆ N ₂ O ₆ U	C ₂₄ H ₁₂ Cl ₆ N ₂ O ₈ U	C ₂₆ H ₁₂ Cl ₆ N ₂ O ₆ U
formula weight	875.09	907.09	899.11
crystal system	monoclinic	monoclinic	triclinic
space group	<i>C2/c</i>	<i>P2₁/c</i>	<i>P-1</i>
a (Å)	14.5255(11)	16.353(2)	7.4075(3)
b (Å)	9.8903(7)	8.7161(11)	9.4093(4)
c (Å)	20.2404(19)	21.513(3)	22.1355(9)
α (deg)	90	90	77.994(3)
β (deg)	107.335(11)	110.042(2)	81.003(3)
γ (deg)	90	90	68.227(4)
V (Å ³)	2775.7(4)	2880.6(6)	1396.09(11)
Z	4	4	2
T (K)	293(2)	100(2)	293(2)
λ (Mo K α)	0.71073	0.71073	0.71073
D_{calc} (g cm $^{-3}$)	2.094	2.092	2.139
μ (mm $^{-1}$)	6.468	6.242	6.434
R_{int}	0.0507	0.0499	0.0370
R1 [$I > 2\sigma(I)$]	0.0274	0.0329	0.0311
wR2 [$I > 2\sigma(I)$]	0.0587	0.0705	0.0634

IV. Additional Figures

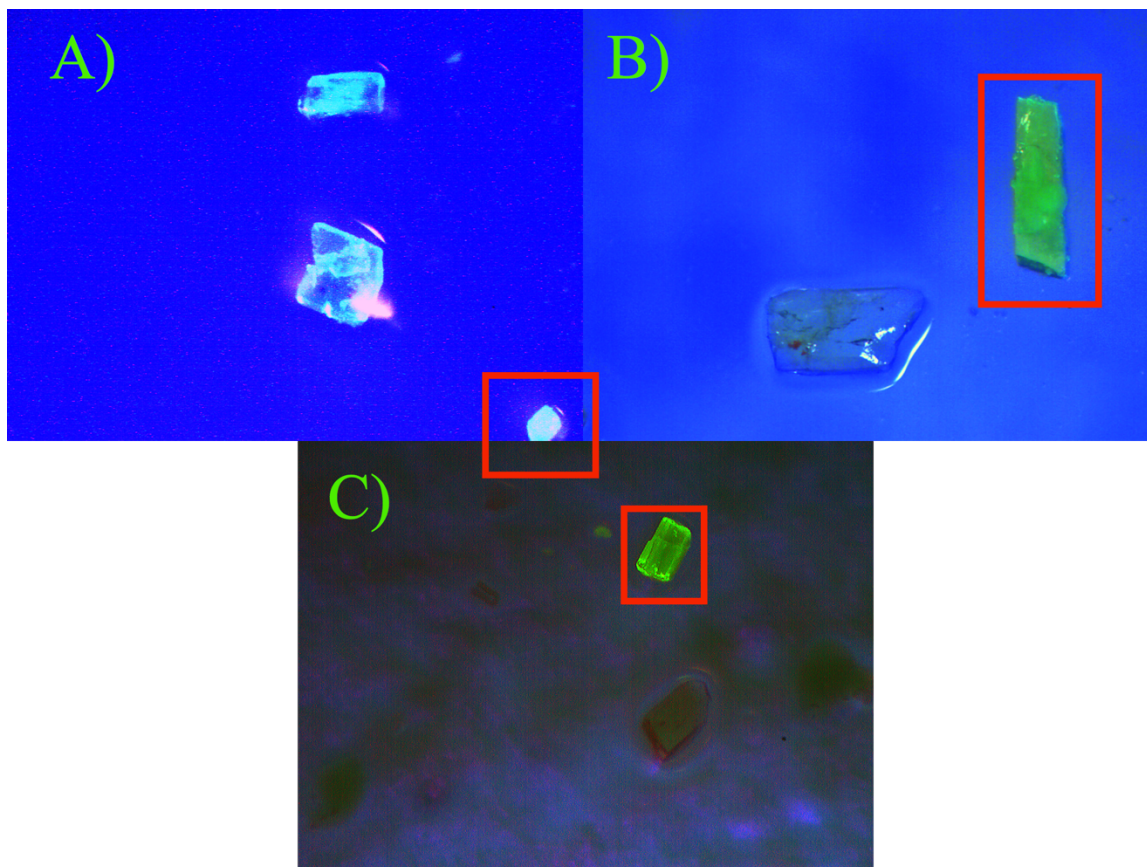


Figure S1 Selection of luminescent ‘bent’ and ‘non-bent’ single crystals of complexes **1-6** upon irradiation by UV light. Differences in crystal color and brightness were used to identify ‘bent’ and ‘non-bent’ phases for **A)** 2,4,6-trifluorobenzoic acid complexes **1** and **4**; **B)** 2,4,6-trichlorobenzoic acid complexes **2** and **5**; **C)** 2,4,6-tribromobenzoic acid complexes **3** and **6**. Crystals of ‘bent’ phases (complexes **1-3**) are shown in red boxes.

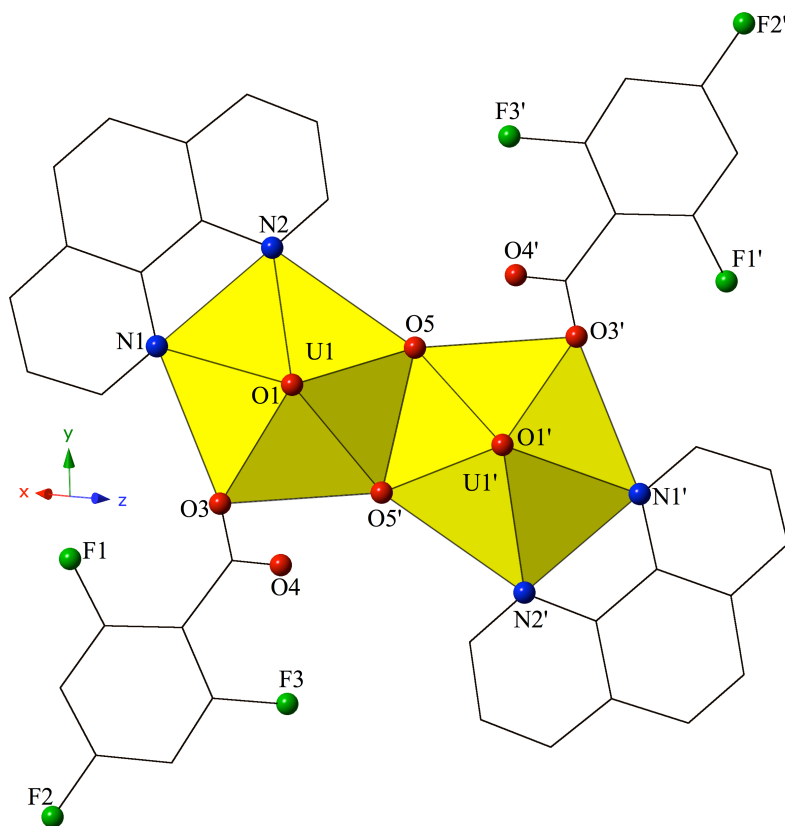


Figure S2 Polyhedral representation of local coordination geometry of **4**. Yellow polyhedra represent uranium metal centers, whereas green, red, and blue spheres represent fluorine, oxygen, and nitrogen atoms, respectively. All H atoms have been omitted for clarity.

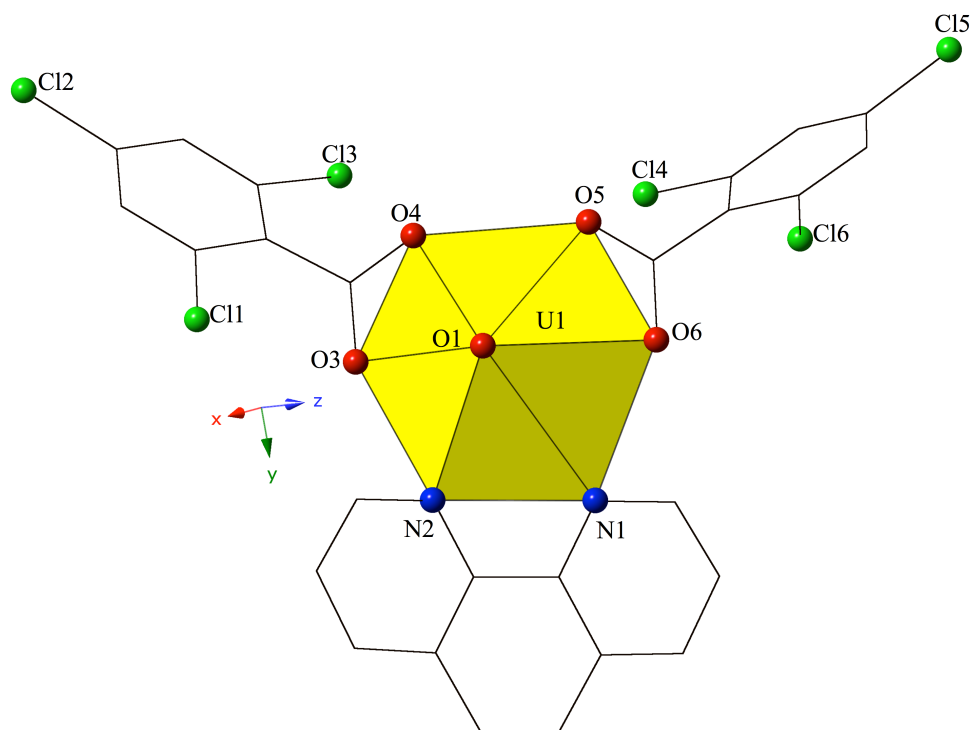


Figure S3 Polyhedral representation of local coordination geometry of **5**. Lime green spheres represent chlorine atoms. Lattice water molecules and all H atoms have been omitted for clarity.

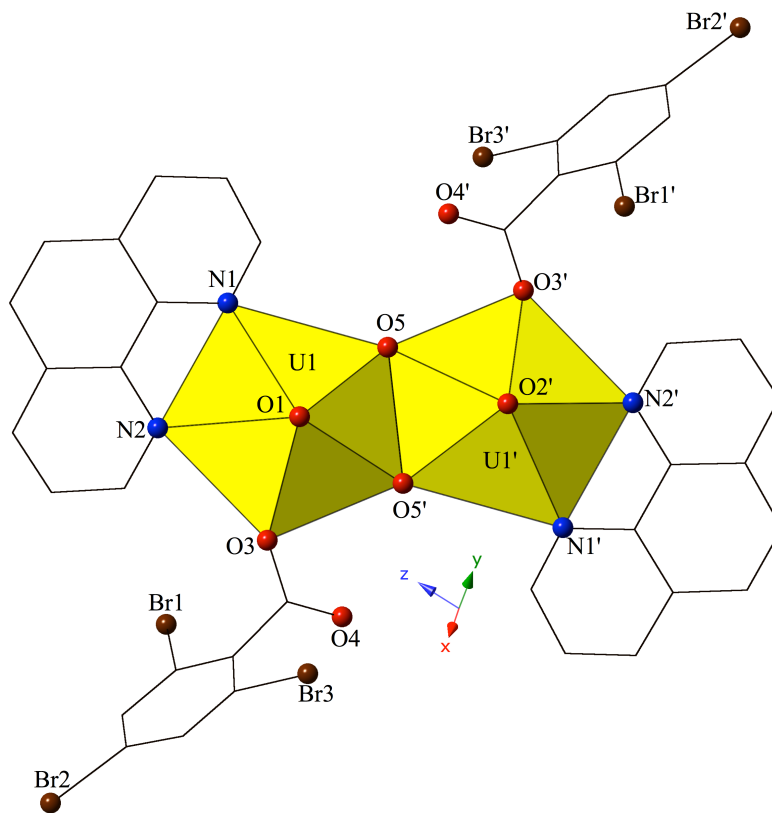


Figure S4 Polyhedral representation of local coordination geometry of **6**. Brown spheres represent chlorine atoms. All H atoms have been omitted for clarity.

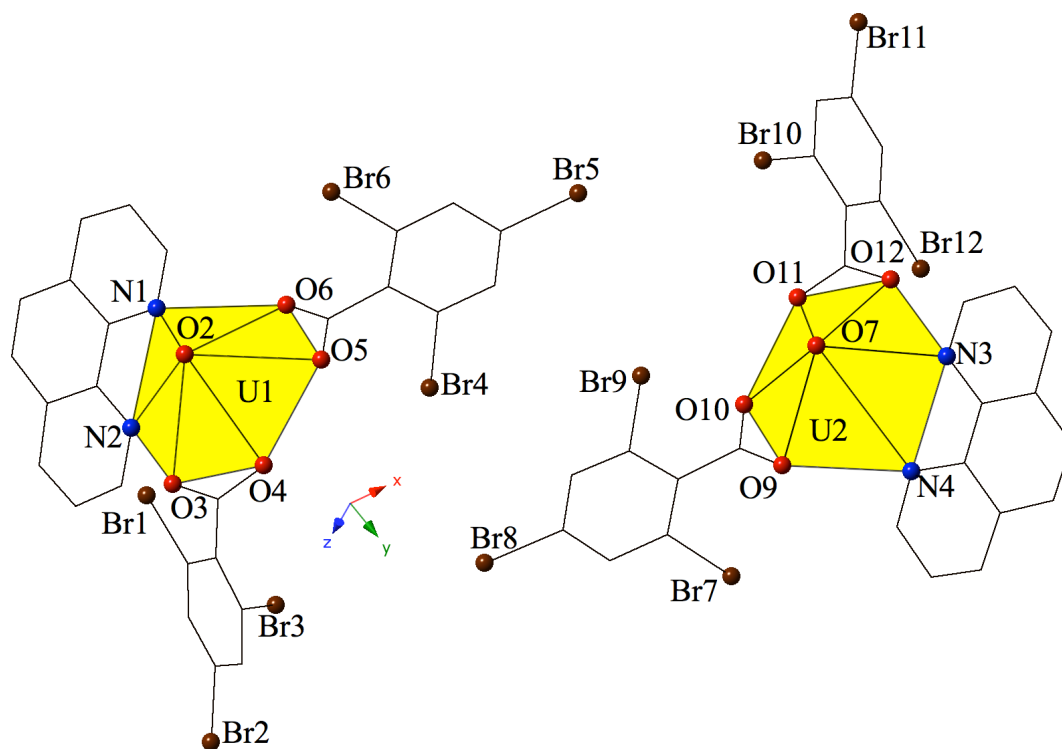


Figure S5 Polyhedral representation of local coordination geometry of **7**. Brown spheres represent chlorine atoms. All H atoms have been omitted for clarity.

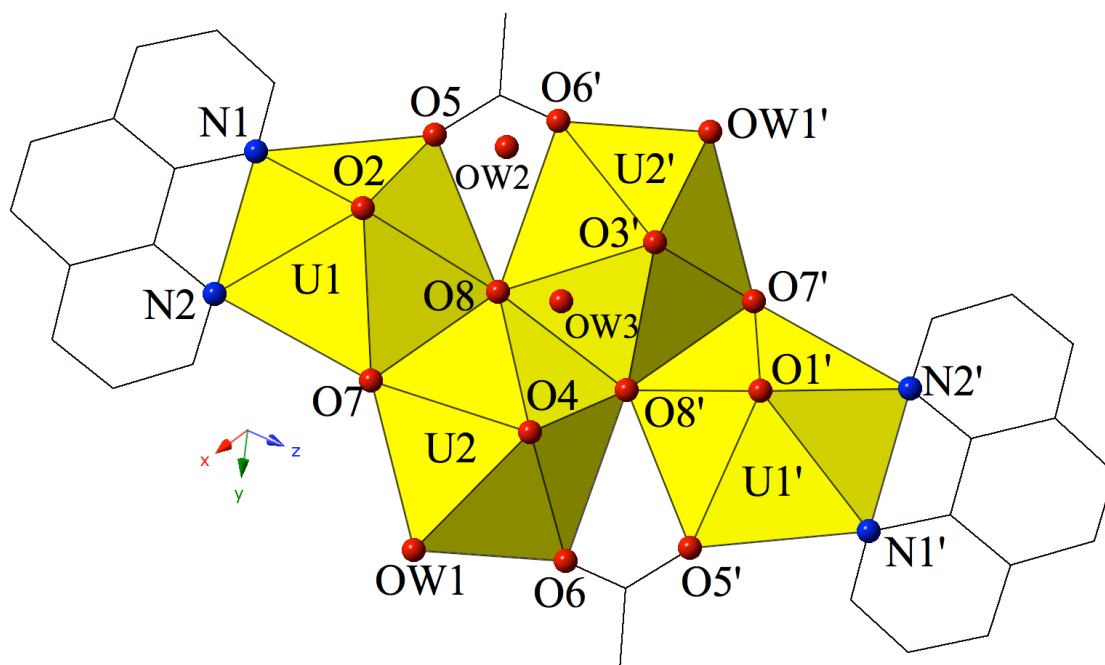


Figure S6 Polyhedral representation of local coordination geometry of **8**. All H atoms have been omitted for clarity.

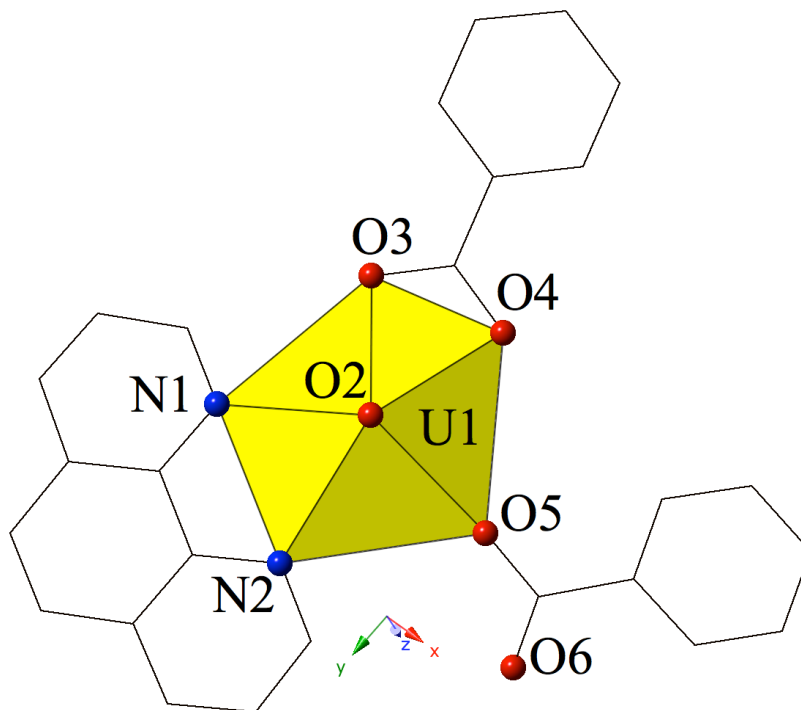


Figure S7 Polyhedral representation of local coordination geometry of **9**. All H atoms have been omitted for clarity.

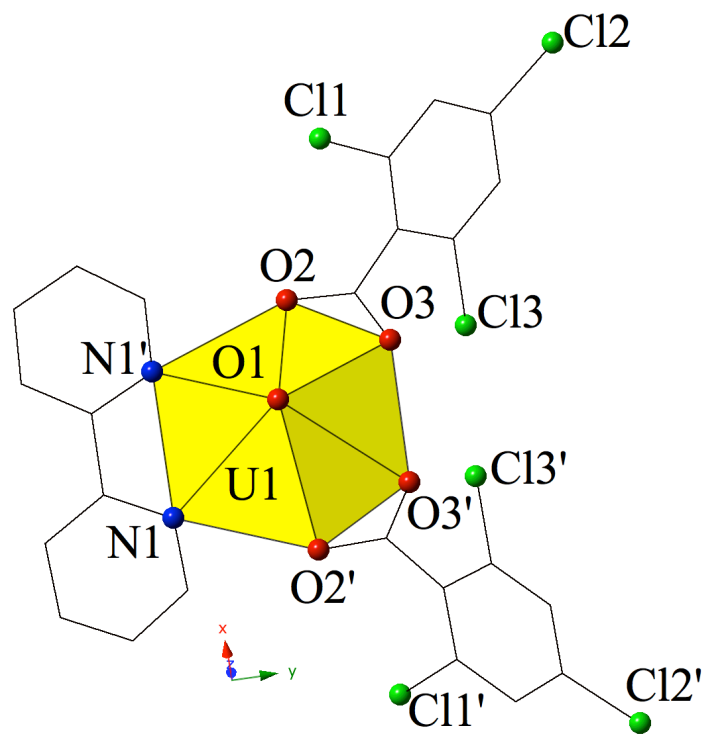


Figure S8 Polyhedral representation of local coordination geometry of **10**. All H atoms have been omitted for clarity.

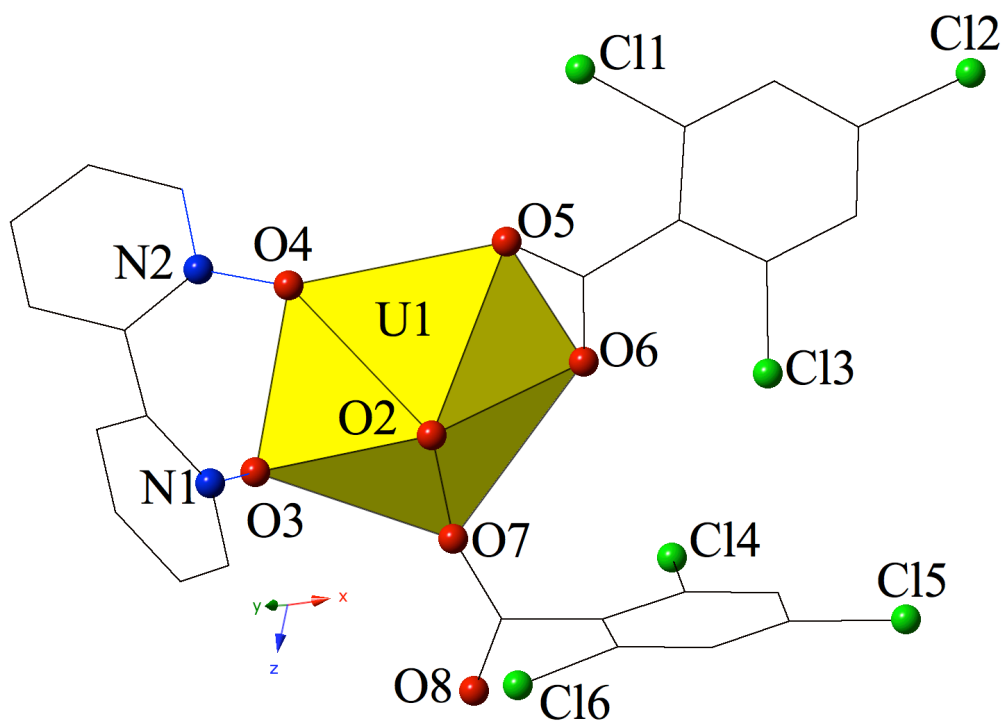


Figure S9 Polyhedral representation of local coordination geometry of **11**. All H atoms have been omitted for clarity.

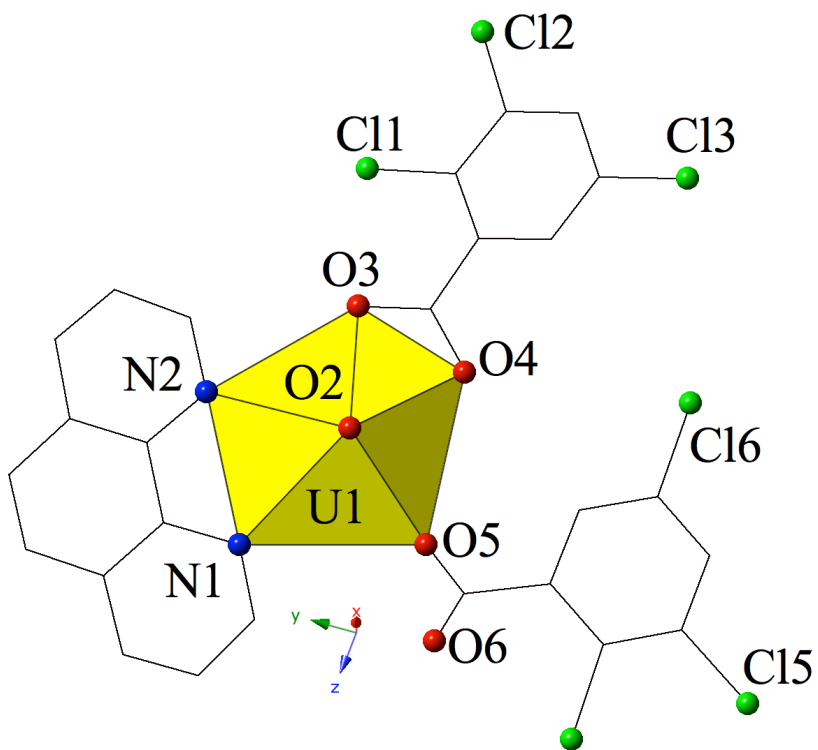


Figure S10 Polyhedral representation of local coordination geometry of **12**. All H atoms have been omitted for clarity.

V. Additional DFT and QTAIM Data

Table S4 Selected structural parameters of complexes **1-3** and simulated 2,4,6-triiodobenzoic acid analogue.

X		U-oxo (Å)	OUO bend (°)	O-H (Å)	U-O _{eq} (Å)	U-N (Å)
F	Exp	1.781	164.94	2.401	2.281	2.613, 2.780
	PBE0	1.761	165.89	2.239	2.264	2.662, 2.860
	B3LYP	1.780	165.62	2.286	2.279	2.695, 2.907
Cl	Exp	1.774	162.87	2.360	2.282	2.665, 2.767
	PBE0	1.760	165.49	2.240	2.264	2.658, 2.850
	B3LYP	1.779	165.26	2.283	2.287	2.700, 2.897
Br	Exp	1.778	162.18	2.317	2.272	2.625, 2.758
	PBE0	1.760	165.46	2.237	2.269	2.660, 2.848
	B3LYP	1.778	165.25	2.278	2.293	2.703, 2.890
I	Exp	-	-	-	-	-
	PBE0	1.759	165.33	2.236	2.275	2.663, 2.844
	B3LYP	1.778	165.22	2.277	2.299	2.707, 2.889

Table S5 Topological properties of the U-oxo bonds in **1-3** and simulated 2,4,6-triiodobenzoic acid analogue, evaluated using B3LYP/def(2)-TZVP derived densities.

X	ρ_{BCP}	$\nabla^2 \rho_{\text{BCP}}$	H_{BCP}	ϵ
free [UO ₂] ²⁺	0.366	0.271	-0.395	0
F	0.297	0.357	-0.257	0.011
Cl	0.298	0.357	-0.258	0.012
Br	0.299	0.357	-0.259	0.013
I	0.299	0.357	-0.260	0.013

U-N bonds were fixed at the experimentally determined separation in order to include aspects of the crystal environment. Whereas fixing the U-N bonds does not simulate the crystal environment completely, it partially accounts for crystal packing effects. In these simulations, other potential origins of the bending (i.e. the presence of neighboring complexes in the condensed phase) were omitted, yet agreement with the experimentally observed trend was obtained, indicating that the close proximity of the ligands coordinating the uranyl is the origin of the uranyl bending. We note that the details of the electronic structure are not strongly influenced by the crystal environment (assuming that the geometrical structure is representative of the bulk phase) as we have demonstrated previously.²

Table S6 Integrated properties of the U-oxo bonds in **1-3**, evaluated using B3LYP/def(2)-TZVP derived densities. * UN bonds were constrained to the experimental values.

X	$q(\text{U})$	$q(\text{O}_{\text{vl}})$	$\delta(\text{U}, \text{O}_{\text{vl}})$	$\lambda(\text{U})$	$\lambda(\text{O})$
free $[\text{UO}_2]^{2+}$					
F	+3.09	-0.91	1.89	26.01	7.75
F*	+3.08	-0.91	1.87	25.99	7.75
Cl	+3.09	-0.91	1.89	26.01	7.75
Cl*	+3.08	-0.91	1.87	25.99	7.74
Br	+3.09	-0.91	1.89	26.01	7.74
Br*	+3.08	-0.91	1.87	25.99	7.74

Table S7 Topological properties of the U-N bonds in **1-3**, evaluated using B3LYP/def(2)-TZVP derived densities. Values in parentheses correspond to non-planar nitrogen centers. * UN bonds were constrained to the experimental values.

X	$\rho_{\text{BCP}}(\text{U}, \text{N})$	$\nabla^2 \rho_{\text{BCP}}(\text{U}, \text{N})$	$H_{\text{BCP}}(\text{U}, \text{N})$
F	0.041 (0.026)	+0.102 (+0.061)	-0.004 (-0.001)
F*	0.049 (0.034)	+0.121 (+0.087)	-0.006 (-0.002)
Cl	0.041 (0.027)	+0.101 (+0.070)	-0.004 (-0.001)
Cl*	0.049 (0.036)	+0.123 (+0.090)	-0.006 (-0.003)
Br	0.040 (0.027)	+0.100 (+0.071)	-0.004 (-0.001)
Br*	0.048 (0.036)	+0.117 (+0.091)	-0.006 (-0.003)

Table S8 Ratios of non-planar nitrogen charges to U-N separations in **1-3**.

X	$Q(\text{N}_{\text{ax}})$ (a.u.)	$r(\text{U}-\text{N}_{\text{ax}})$ (Å / a.u.)	Q / r
F	-1.15	2.780 / 5.255	-0.219
Cl	-1.15	2.767 / 5.231	-0.220
Br	-1.15	2.758 / 5.213	-0.226

Table S9 Relative energies of linearly constrained structures to those in which U-N bond lengths are held at experimental values. Values are given in eV (kJ/mol).

X	ΔE
F	-0.063 (-6.1)
Cl	-0.099 (-9.6)
Br	-0.119 (-11.5)

In Table S9, the energies of linearized complexes are compared to optimized complexes in which the U-N bonds were held fixed at the experimental geometry, giving O-U-O angles of 164.11, 163.02 and 162.24° for the fluoro-, chloro- and bromo- complexes, respectively. These latter structures correspond to local energetic minima (subject to the constraints imposed) and therefore energy differences give a clear indication of the energy gained by the uranyl bending to the minimum energy geometry in each case.

VI. Vibrational and Luminescence Spectroscopy Data

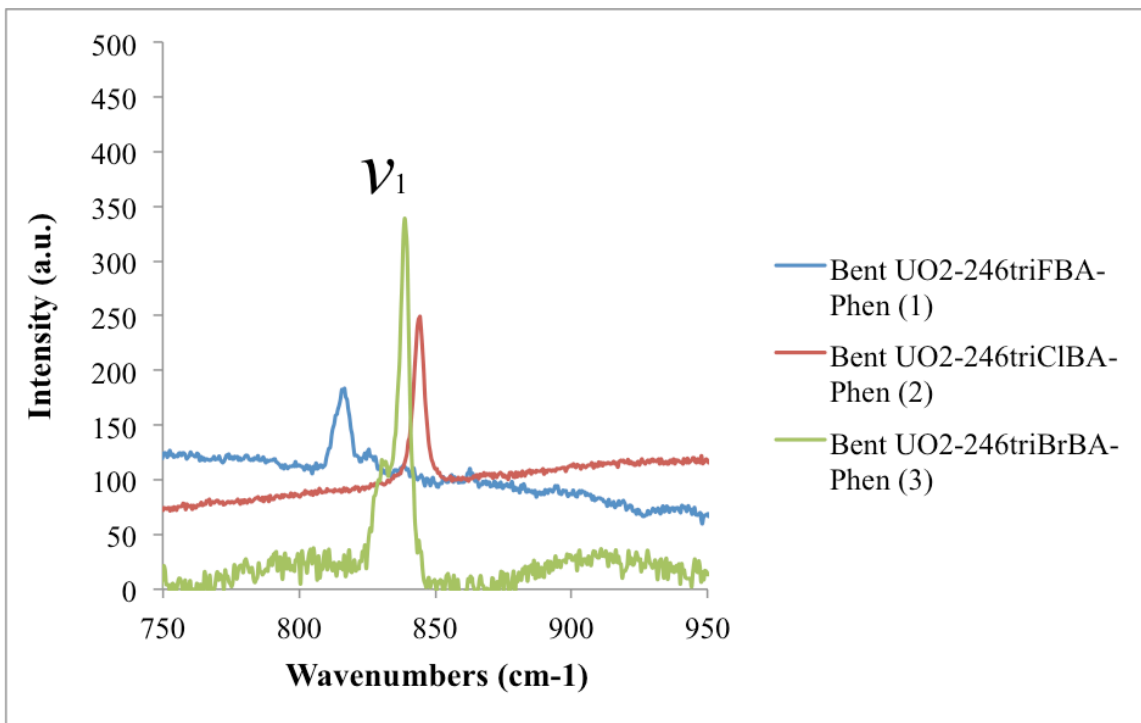


Figure S11 Raman spectra of ‘bent’ uranyl-2,4,6-trihalobenzoic-phen complexes (1-3). Symmetric stretch (ν_1) of the uranyl cation is highlighted for each complex.

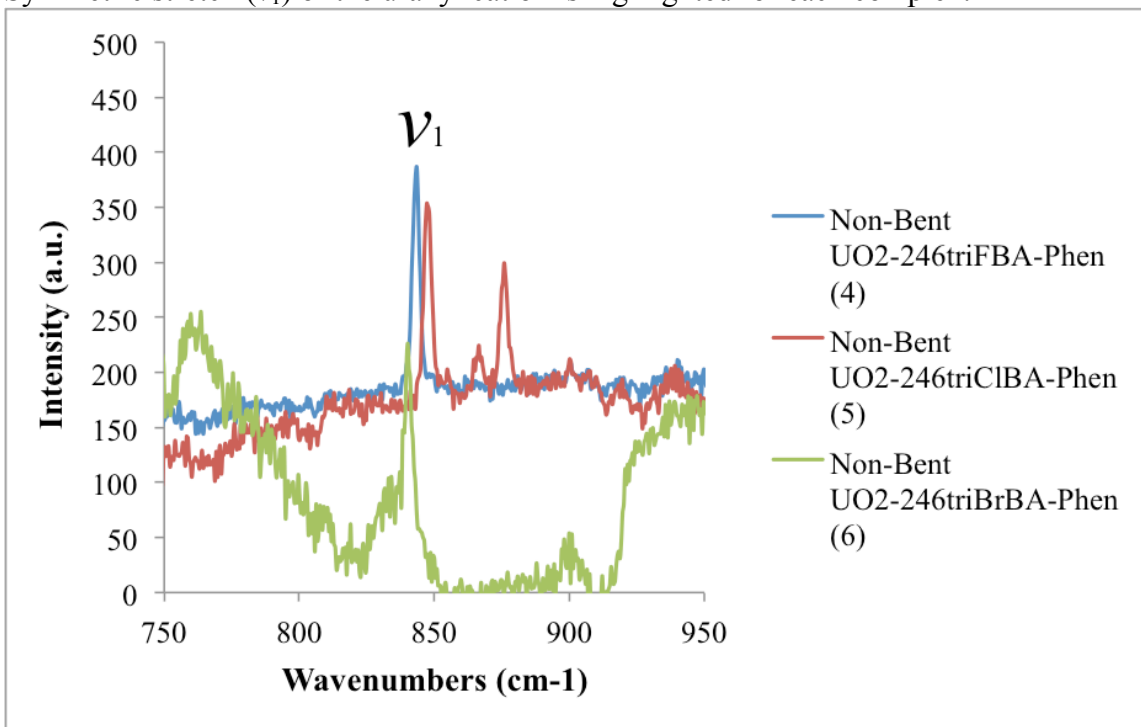


Figure S12 Raman spectra of ‘non-bent’ uranyl-2,4,6-trihalobenzoic-phen complexes (4-6). Symmetric stretch (ν_1) of the uranyl cation is highlighted for each complex.

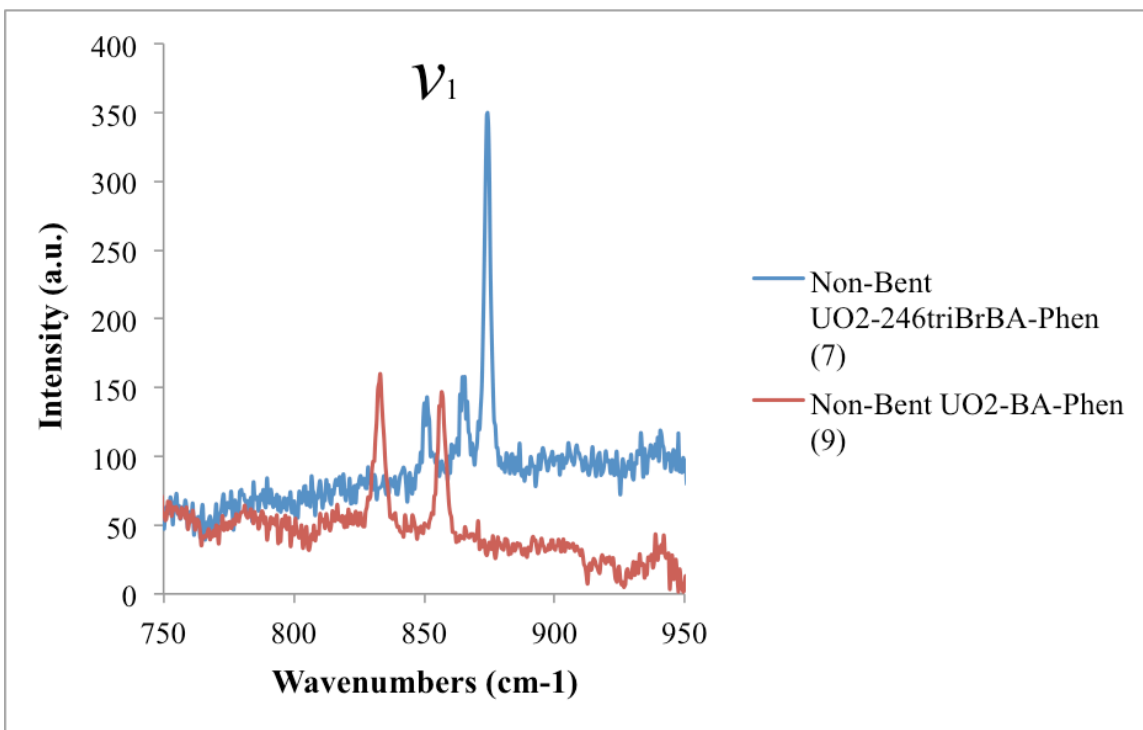


Figure S13 Raman spectra of additional uranyl-2,4,6-tribromobenzoic-phen complex (7) as well as uranyl-benzoic-phen complex (9). Symmetric stretch (ν_1) of the uranyl cation is highlighted for both complexes.

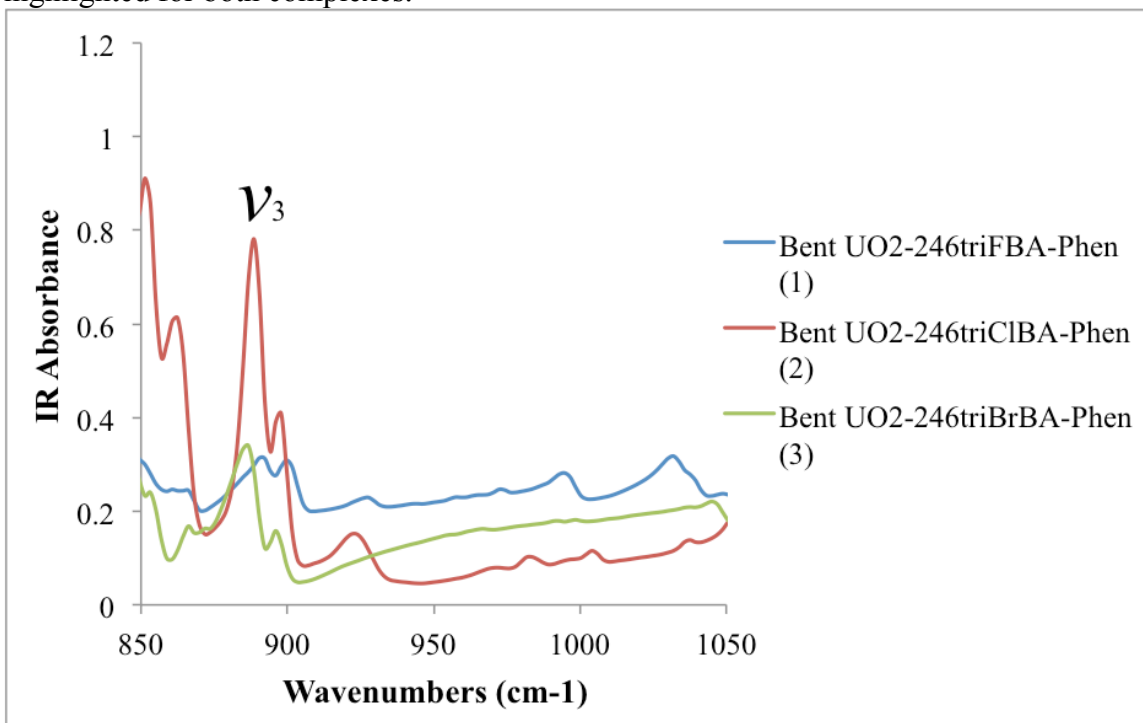


Figure S14 IR spectra of ‘bent’ uranyl-2,4,6-trihalobenzoic-phen complexes (1-3). Asymmetric stretch (ν_3) of the uranyl cation is highlighted for each complex.

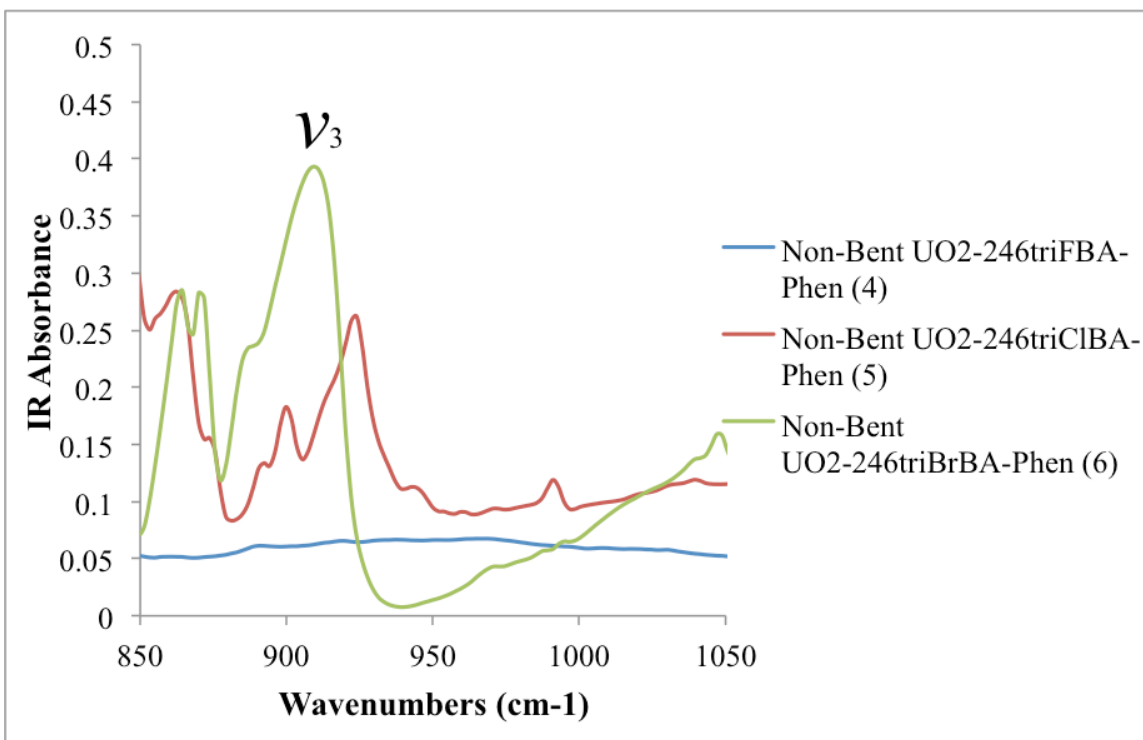


Figure S15 IR spectra of 'non-bent' uranyl-2,4,6-trihalobenzoic-phen complexes (**4-6**). Asymmetric stretch (ν_3) of the uranyl cation is highlighted for each complex.

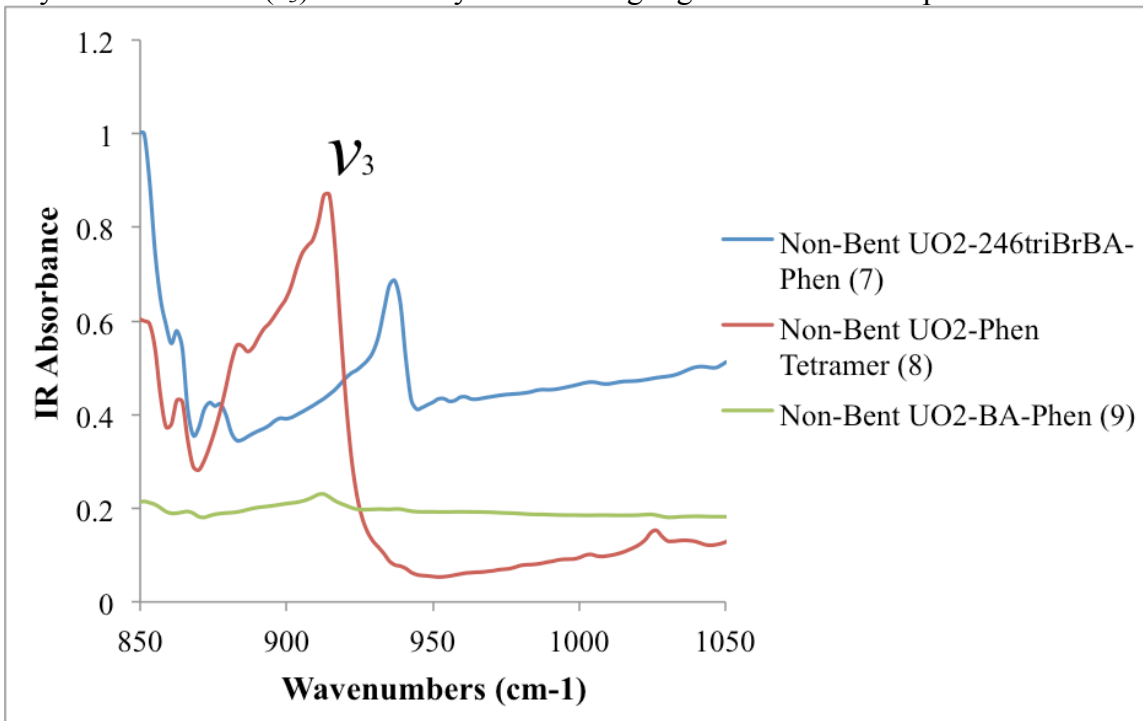


Figure S16 IR spectra of additional uranyl-2,4,6-tribromobenzoic-phen complex (**7**) as well as uranyl-benzoic-phen complexes (**8** and **9**). Asymmetric stretch (ν_3) of the uranyl cation is highlighted for each complex.

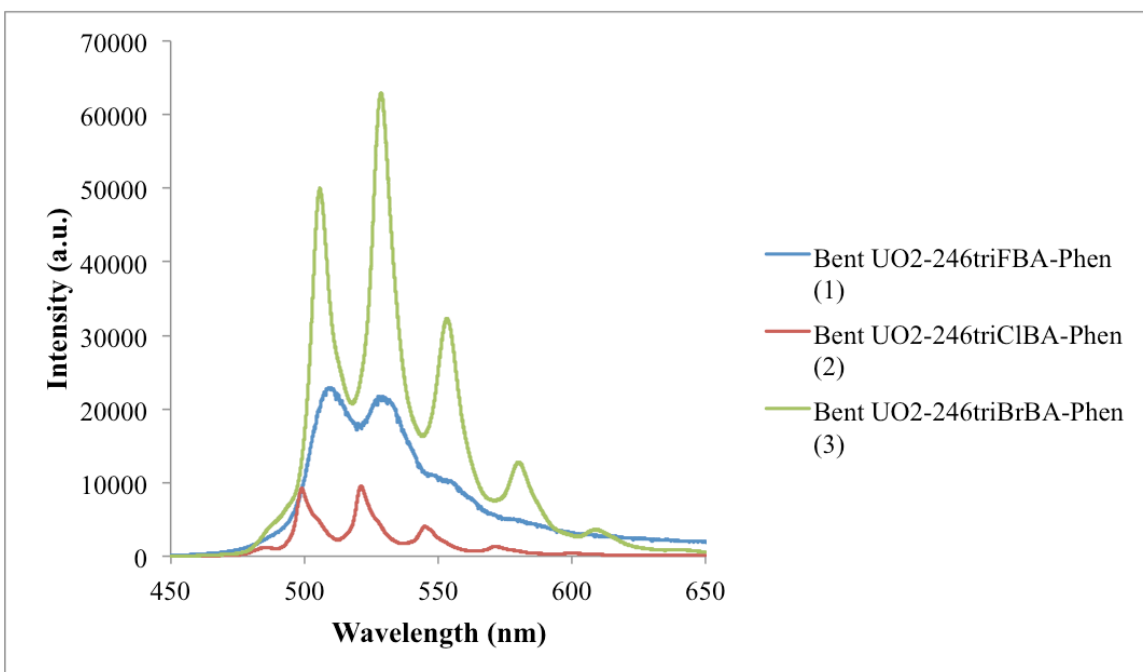


Figure S17 Room temperature, solid-state emission spectra of ‘bent’ uranyl-2,4,6-trihalobenzoic-phen complexes (1-3).

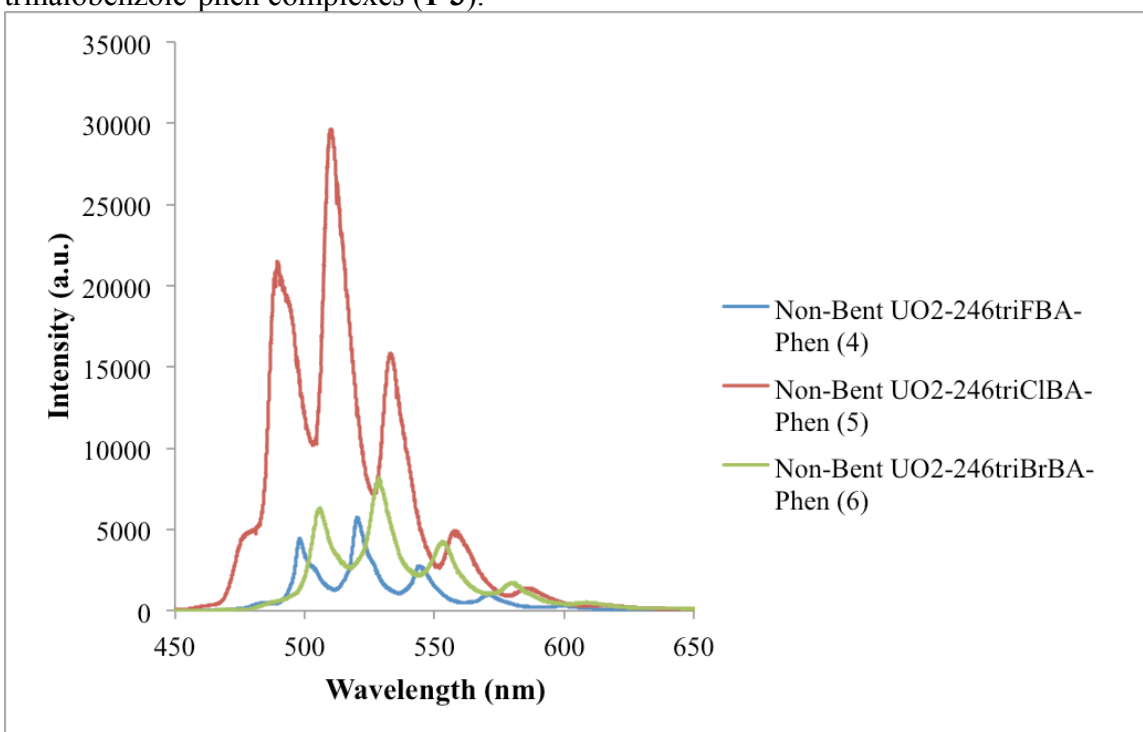


Figure S18 Room temperature, solid-state emission spectra of ‘non-bent’ uranyl-2,4,6-trihalobenzoic-phen complexes (4-6).

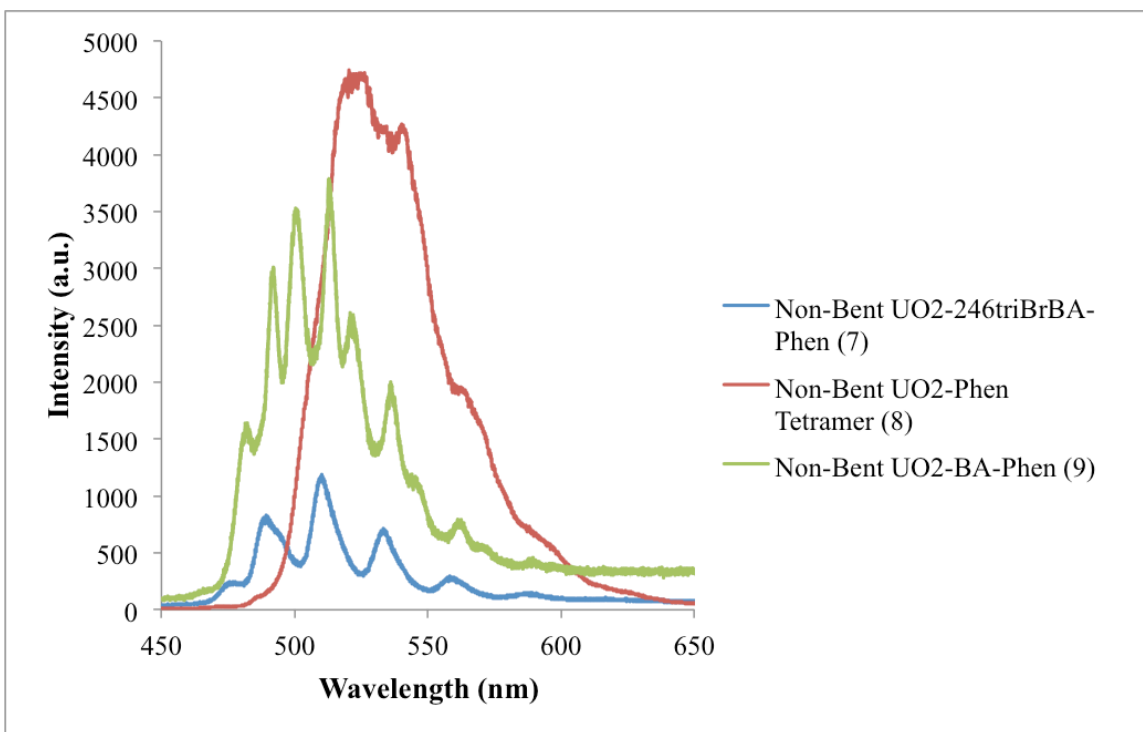


Figure S19 Room temperature, solid-state emission spectra of additional uranyl-2,4,6-tribromobenzoic-phen complex (7) as well as uranyl-benzoic-phen complexes (8 and 9).

VII. Powder X-ray diffraction data

For complexes **8** and **9** it is important to note that calculated patterns are from low temperature (100(2) K) data collections, whereas observed patterns were collected at room temperature (298(2) K). This difference may result in slight shifts in two-theta values.

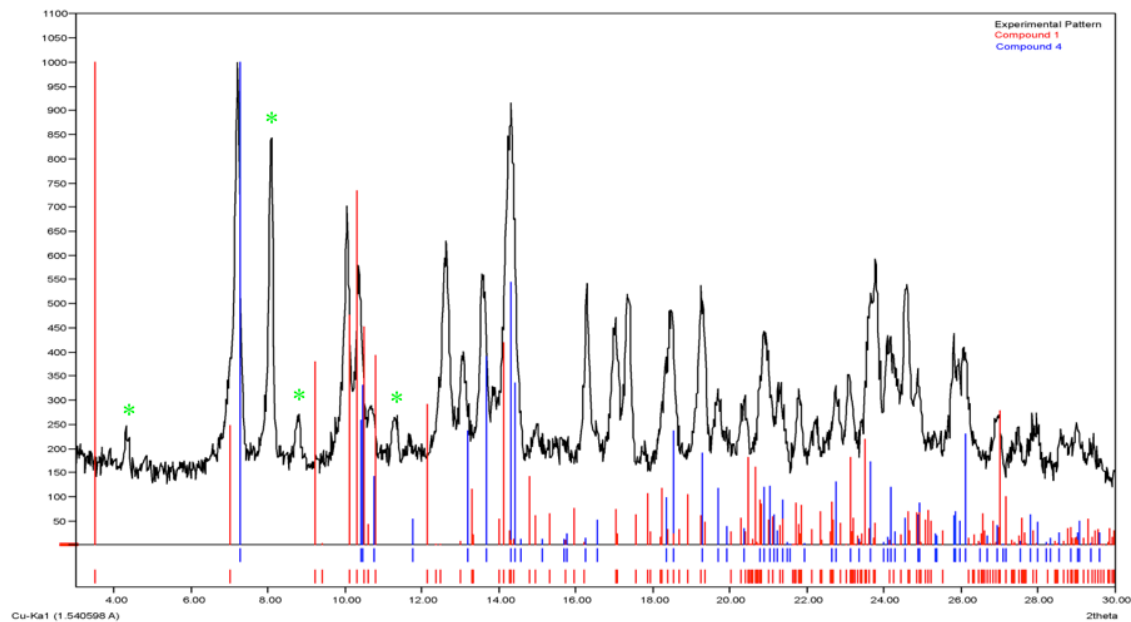


Figure S20 The observed PXRD pattern of complex **1** with calculated pattern overlaid in red. The calculated pattern of complex **5** is also overlaid in blue. Remaining impurities in the bulk product of **1** are highlighted with green asterisks.

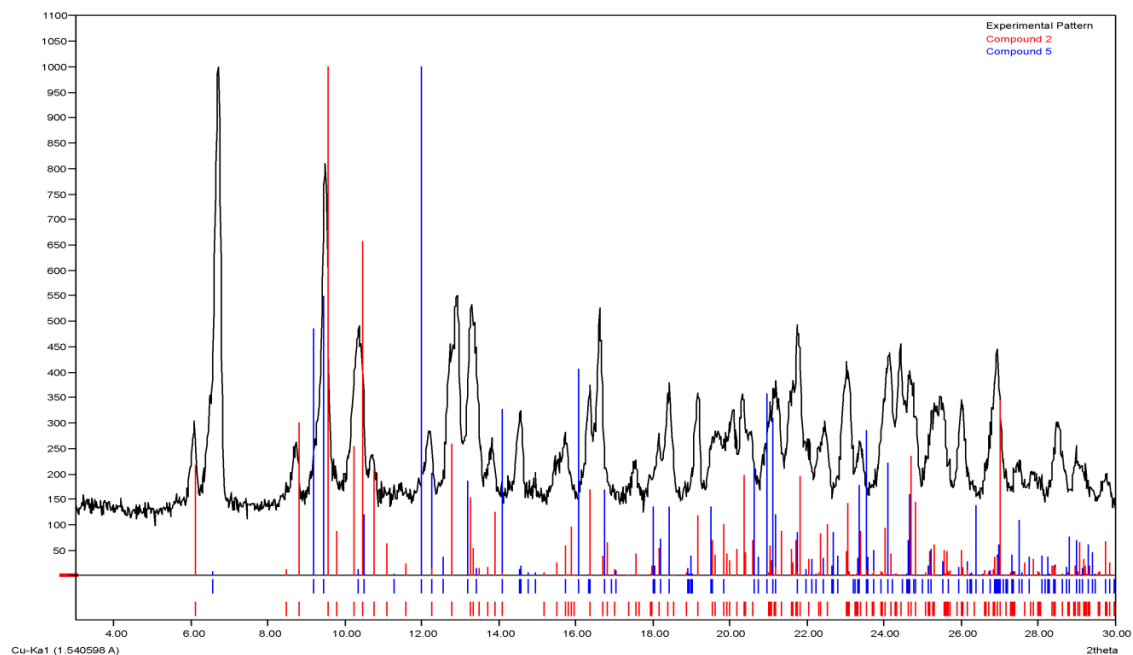


Figure S21 The observed PXRD pattern of complex **2** with calculated pattern overlaid in red. The calculated pattern of complex **5** is also overlaid in blue.

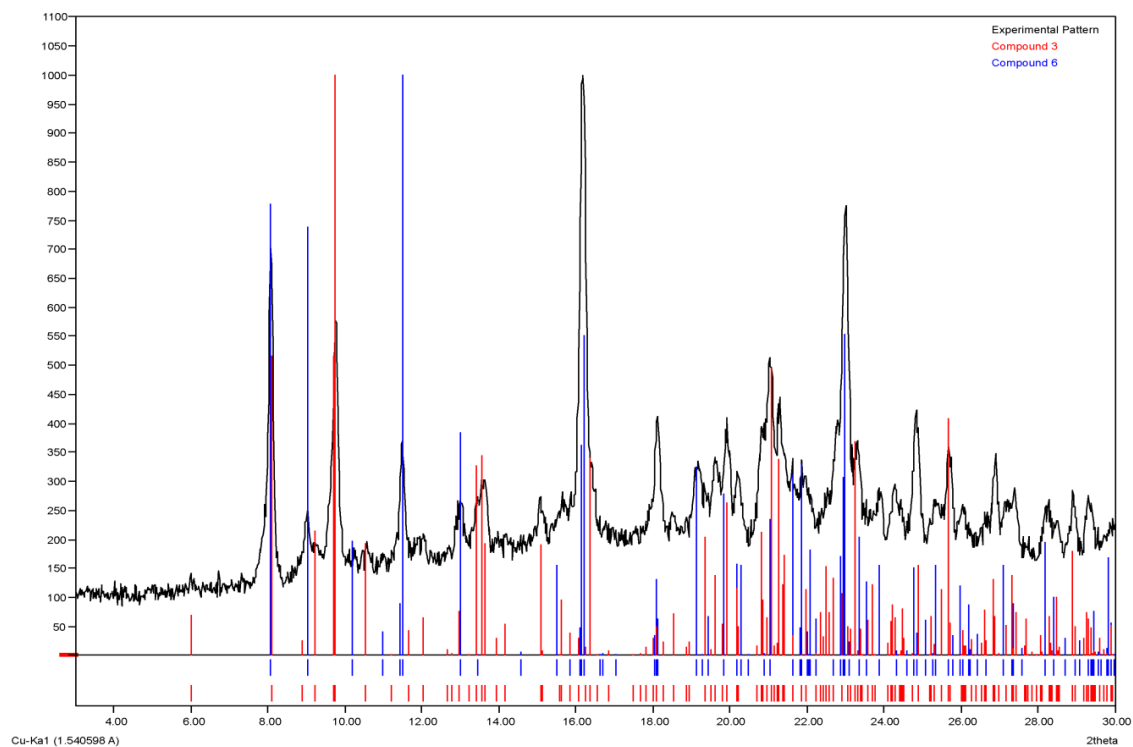


Figure S22 The observed PXRD pattern of complex **3** with calculated pattern overlaid in red. The calculated pattern of complex **6** is also overlaid in blue.

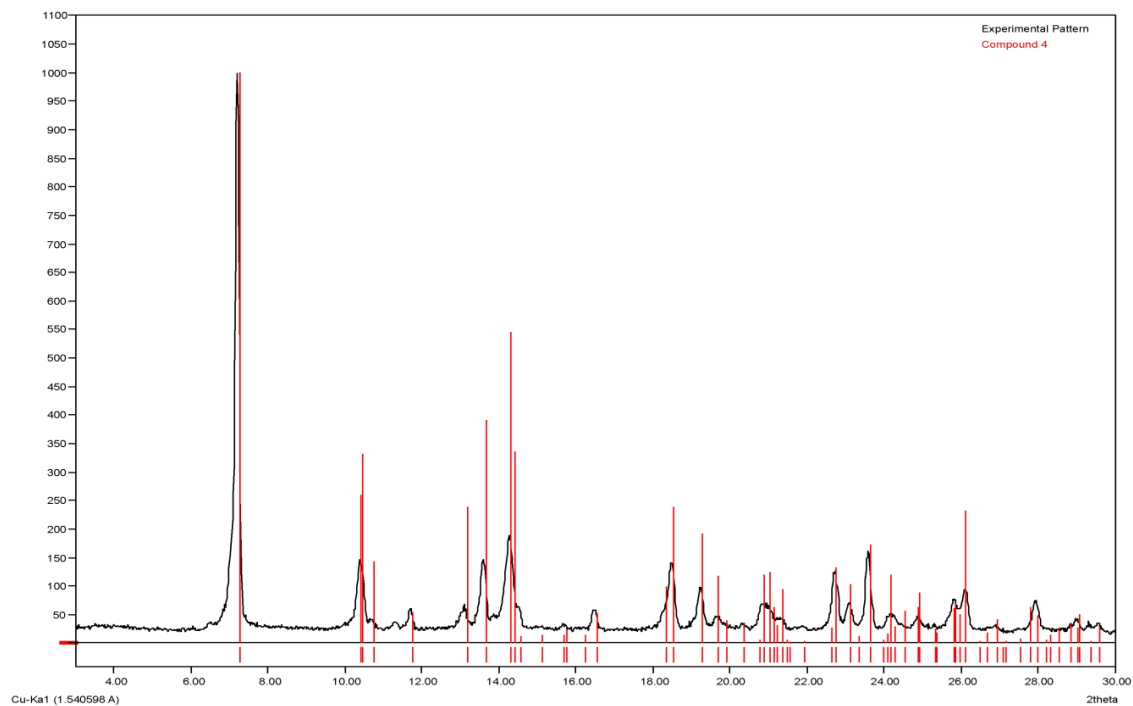


Figure S23 The observed PXRD pattern of complex **4** with calculated pattern overlaid in red.

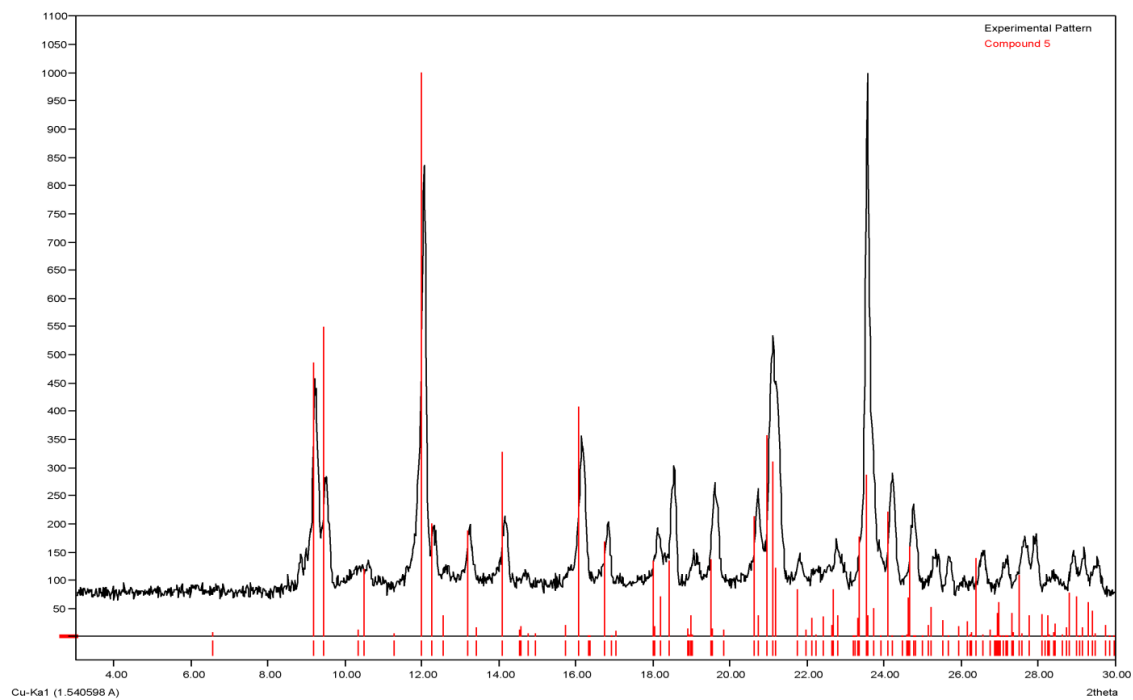


Figure S24 The observed PXRD pattern of complex **5** with calculated pattern overlaid in red.

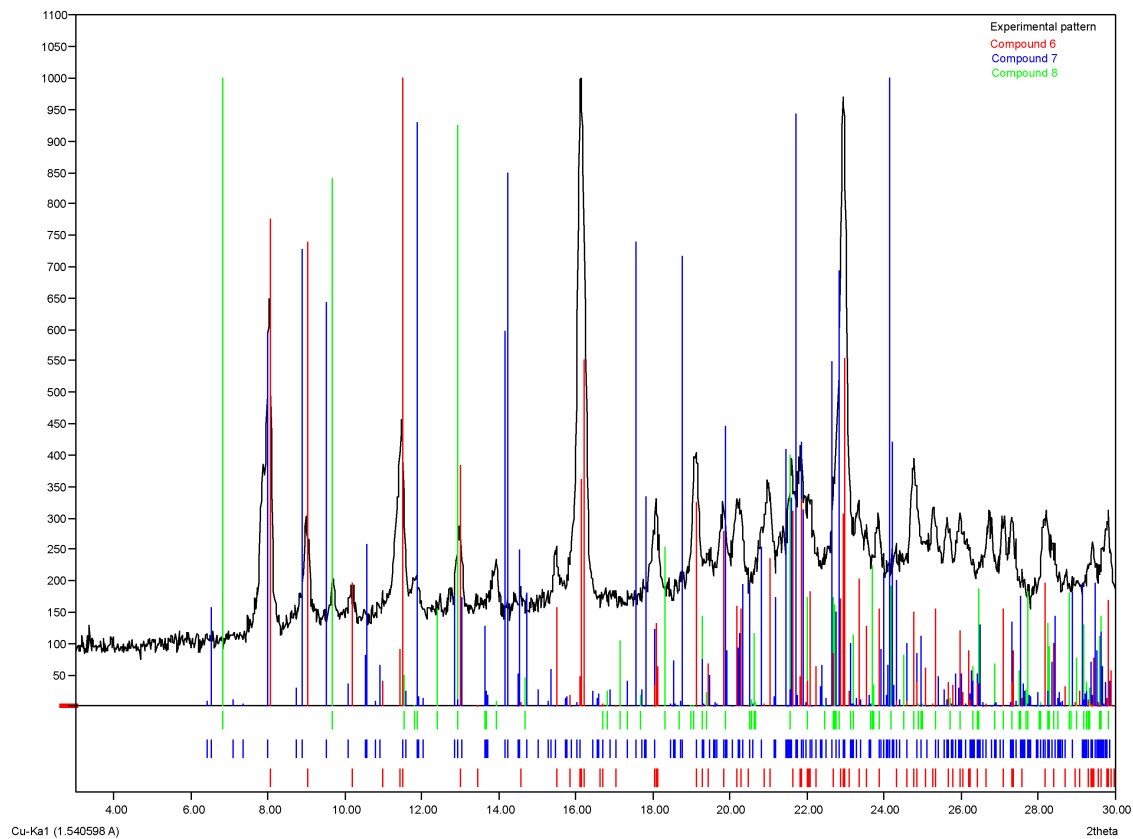


Figure S25 The observed PXRD pattern of complex **6** with calculated pattern overlaid in red. The calculated pattern of complexes **7** and **8** are also overlaid in blue in green, respectively.

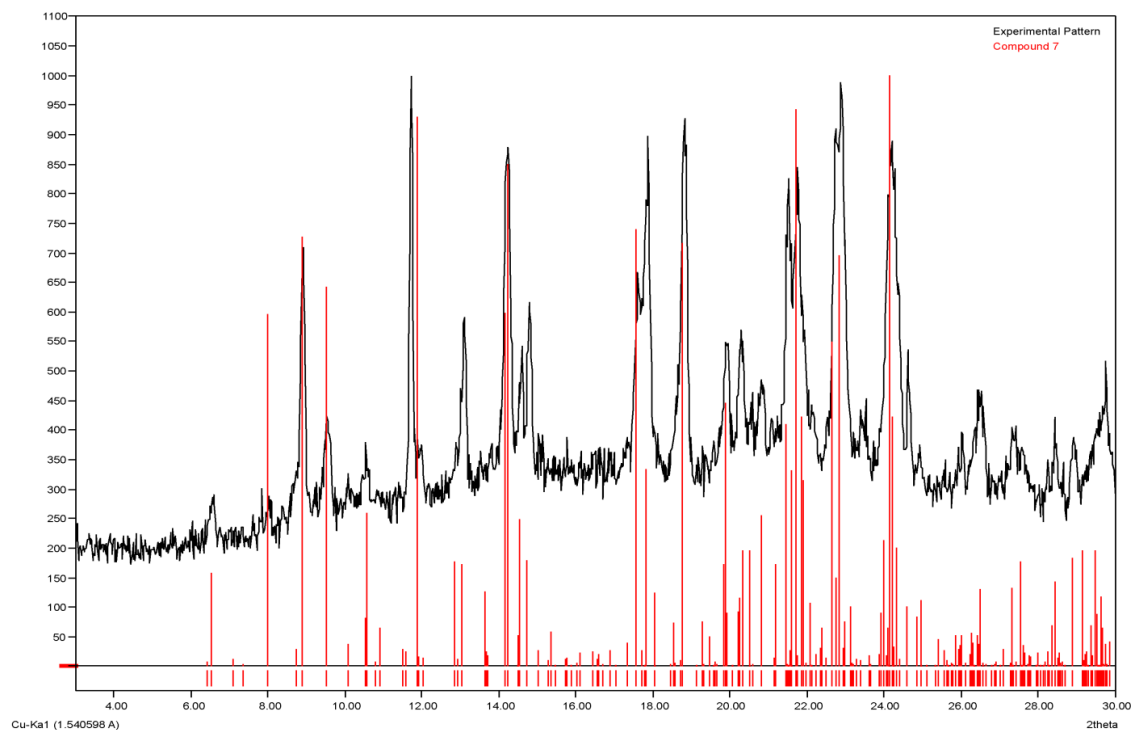


Figure S26 The observed PXRD pattern of complex **7** with calculated pattern overlaid in red.

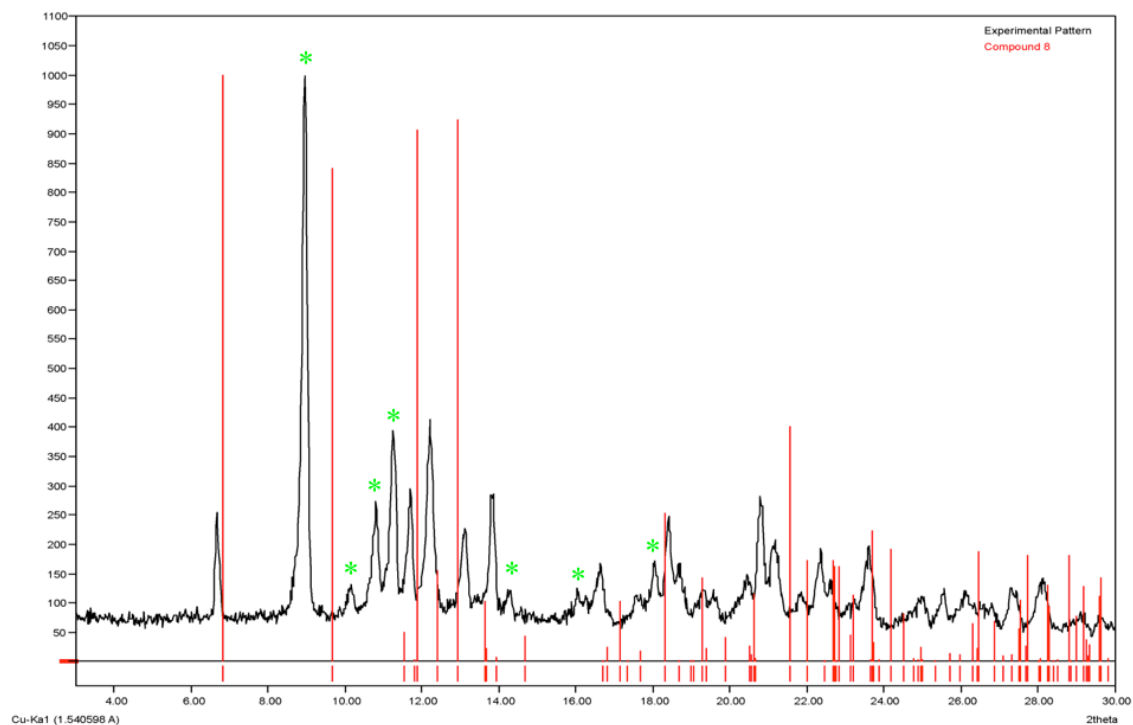


Figure S27 The observed PXRD pattern of complex **8** with calculated pattern overlaid in red. We acknowledge a number of unidentified impurities as highlighted by green asterisks

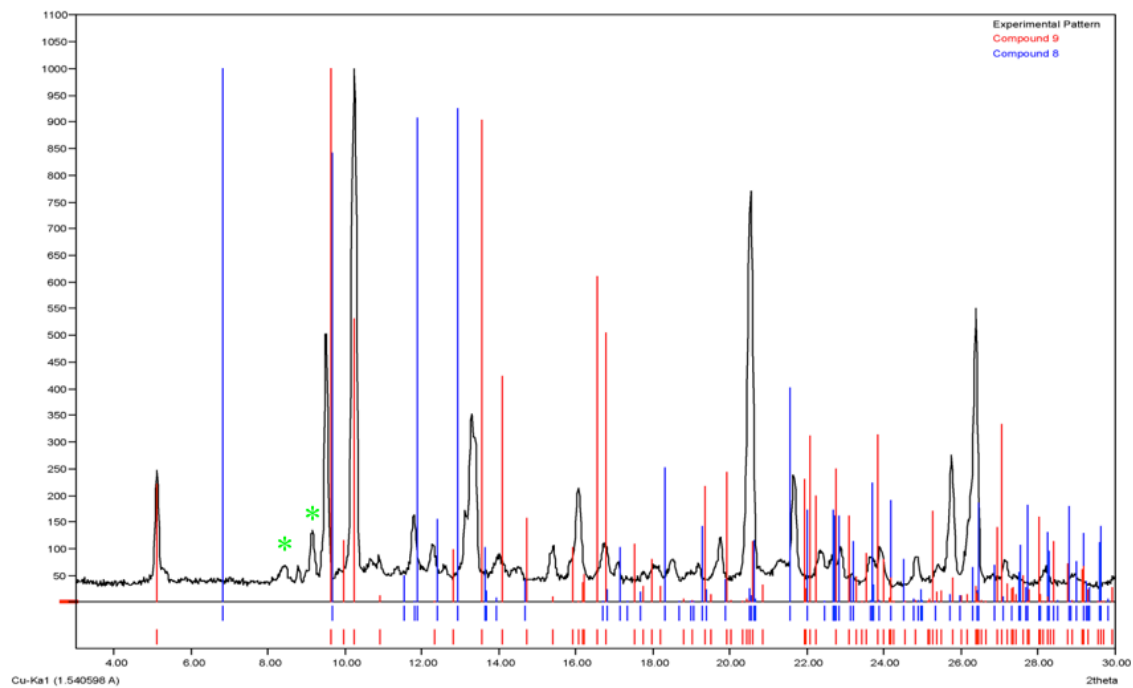


Figure S28 The observed PXRD pattern of complex **9** with calculated pattern overlaid in red. The calculated pattern of complex **8** is also overlaid in blue. Remaining impurities in the bulk product of **9** are highlighted with green asterisks.

VIII. Thermal Ellipsoid Plots

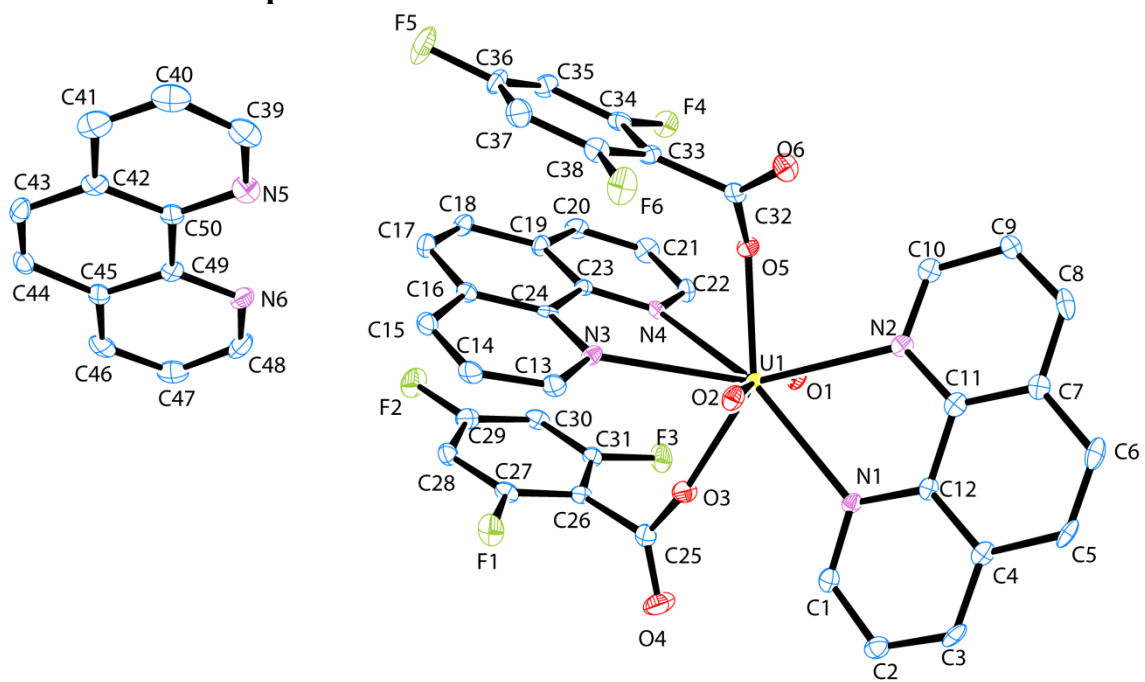
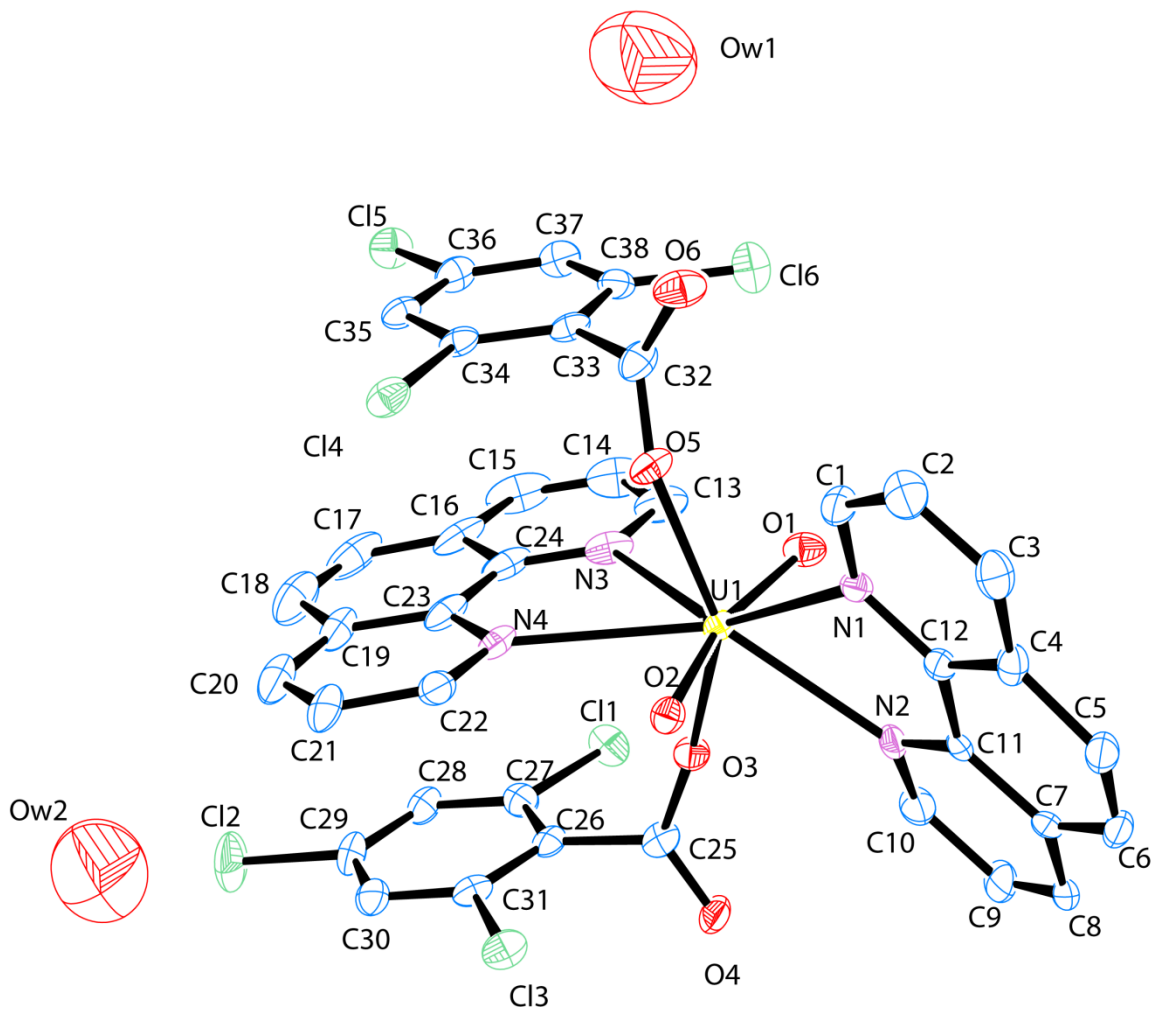


Figure S29 ORTEP illustration of complex 1. Ellipsoids are shown at 50% probability level.



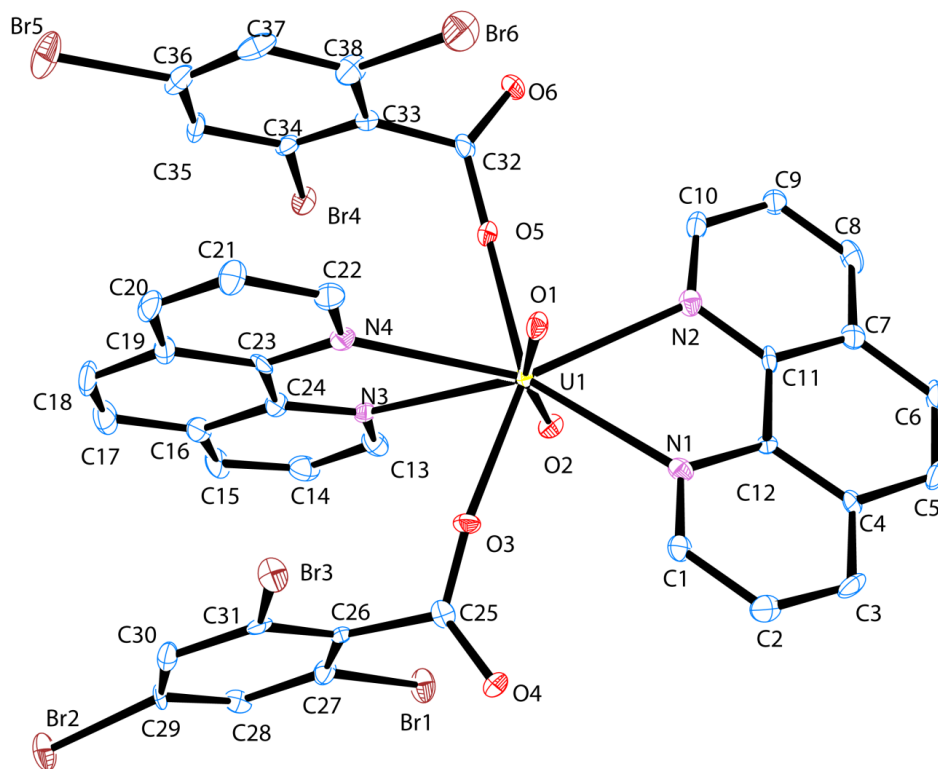


Figure S31 ORTEP illustration of complex **3**. Ellipsoids are shown at 50% probability level.

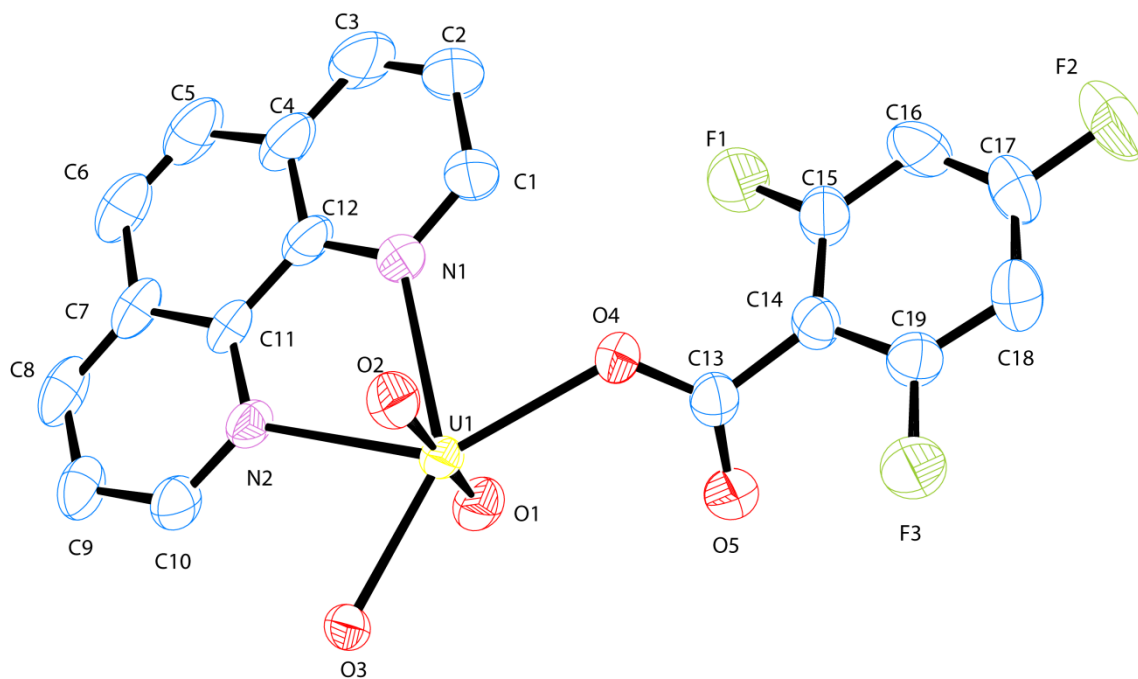


Figure S32 ORTEP illustration of complex **4**. Ellipsoids are shown at 50% probability level.

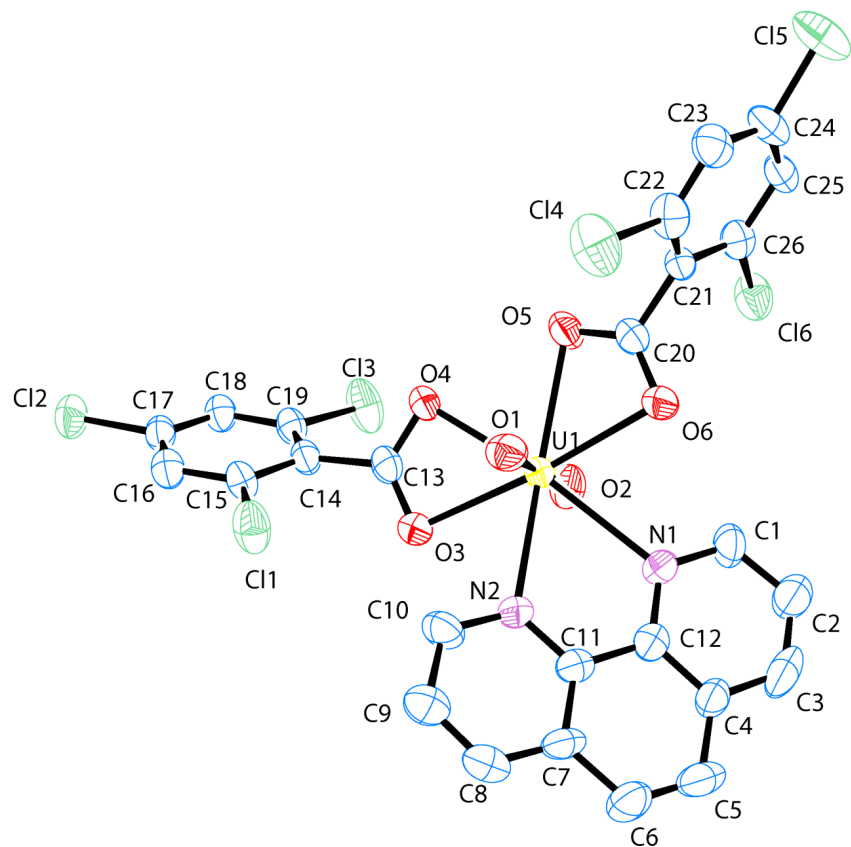


Figure S33 ORTEP illustration of complex **5**. Ellipsoids are shown at 50% probability level.

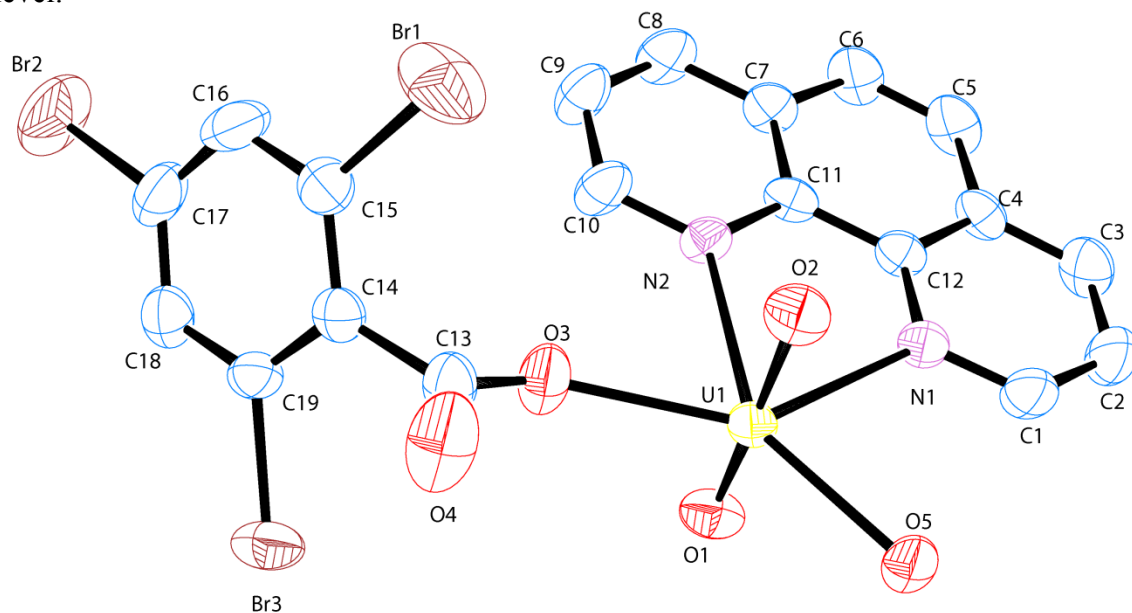


Figure S34 ORTEP illustration of complex **6**. Ellipsoids are shown at 50% probability level.

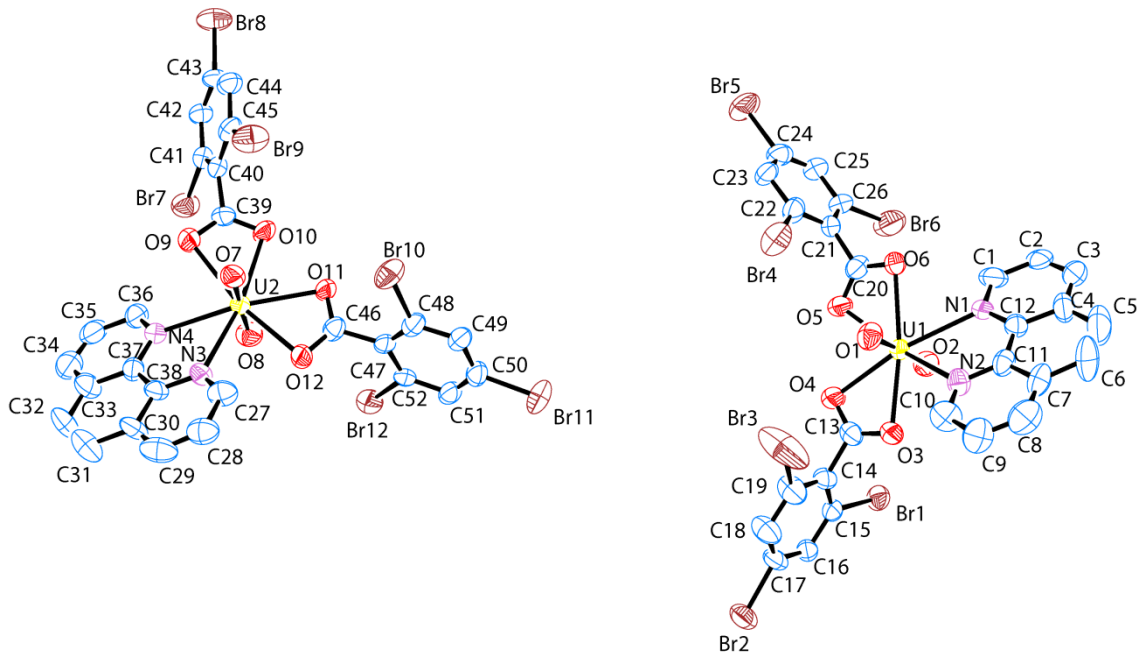


Figure S35 ORTEP illustration of complex **7**. Ellipsoids are shown at 50% probability level.

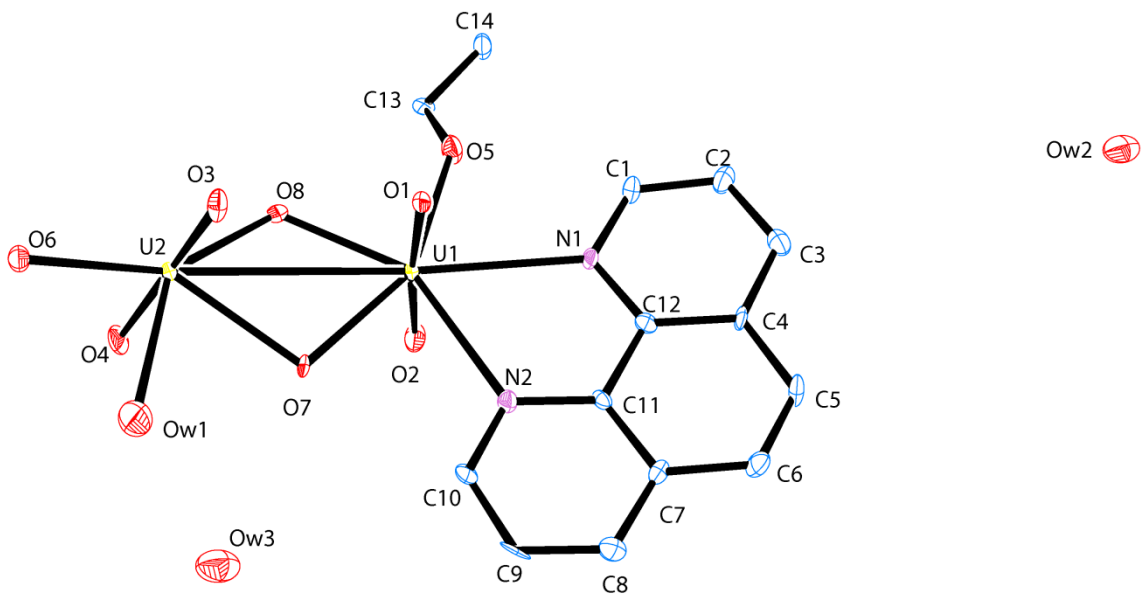


Figure S36 ORTEP illustration of complex **8**. Ellipsoids are shown at 50% probability level.

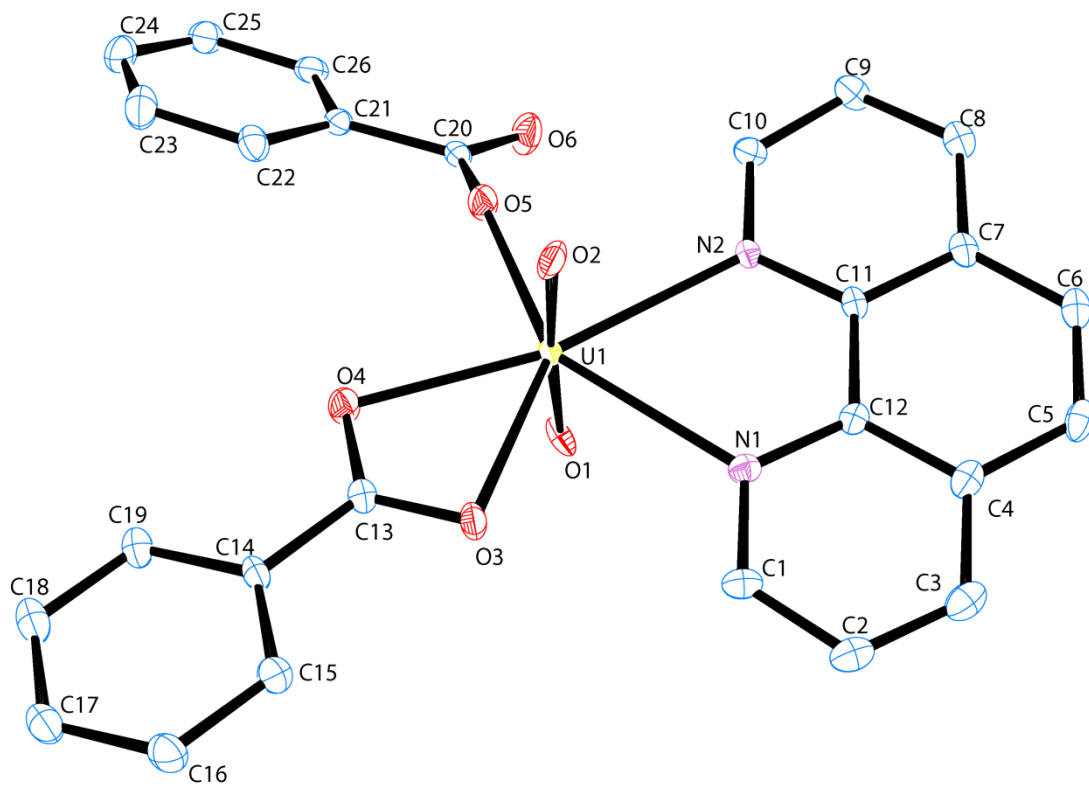


Figure S37 ORTEP illustration of complex **9**. Ellipsoids are shown at 50% probability level.

IX. Tables of Bond Distances and Bond Angles

Table S10 U-O Axial Bond Lengths in Non-Bent UO_2^{2+} complexes (4-9)

Complex	$d_{\text{U1-O1}}$ [Å]	$d_{\text{U1-O2}}$ [Å]	$d_{\text{U2-O3}}$ [Å]	$d_{\text{U2-O4}}$ [Å]	$d_{\text{U2-O7}}$ [Å]	$d_{\text{U2-O8}}$ [Å]
4	1.760(3)	1.764(3)				
5	1.764(4)	1.757(4)				
6	1.765(3)	1.764(4)				
7	1.745(5)	1.748(5)			1.748(5)	1.747(5)
8	1.788(4)	1.800(4)	1.783(4)	1.803(4)		
9	1.7794(19)	1.770(2)				

Table S11 U1-O Equatorial Bond Lengths in Non-Bent UO_2^{2+} complexes (4-9)

Complex	$d_{\text{U1-O3}}$ [Å]	$d_{\text{U1-O4}}$ [Å]	$d_{\text{U1-O5}}$ [Å]	$d_{\text{U1-O5'}}$ [Å]	$d_{\text{U1-O6}}$ [Å]	$d_{\text{U1-O7}}$ [Å]	$d_{\text{U1-O8}}$ [Å]
4	2.385(3)		2.289(3)	2.362(2)			
5	2.486(4)	2.476(4)	2.508(4)		2.468(4)		
6	2.316(3)		2.290(3)	2.361(3)			
7	2.447(5)	2.464(5)	2.476(5)	2.524(5)			
8			2.373(4)			2.298(4)	2.240(4)
9	2.4210(19)	2.397(2)	2.231(2)				

Table S12 U2-O Equatorial Bond Lengths in Non-Bent UO_2^{2+} complexes (7 and 8)

Complex	$d_{\text{U2-O6}}$ [Å]	$d_{\text{U2-O7}}$ [Å]	$d_{\text{U2-O8}}$ [Å]	$d_{\text{U2-O8'}}$ [Å]	$d_{\text{U2-OW1}}$ [Å]	$d_{\text{U2-O9}}$ [Å]	$d_{\text{U2-O10}}$ [Å]	$d_{\text{U2-O11}}$ [Å]	$d_{\text{U2-O12}}$ [Å]
7						2.505 (5)	2.476 (4)	2.475 (5)	2.454 (5)
8	2.424 (4)	2.387 (4)	2.317 (4)	2.249 (4)	2.541 (5)				

Table S13 U-N Bond Lengths in Non-Bent UO_2^{2+} complexes (4-9)

Complex	$d_{\text{U1-N1}}$ [Å]	$d_{\text{U1-N2}}$ [Å]	$d_{\text{U2-N3}}$ [Å]	$d_{\text{U2-N4}}$ [Å]
4	2.613(3)	2.622(3)		
5	2.644(4)	2.618(4)		
6	2.633(4)	2.642(3)		
7	2.641(6)	2.633(6)	2.628(6)	2.638(6)
8	2.675(5)	2.655(5)		
9	2.603(2)	2.565(2)		

Table S14 O-U-O (Axial) and N-U-N Bond Angles in Non-Bent UO_2^{2+} complexes (4-9)

Complex	$\angle\text{O-U1-O}$ [deg]	$\angle\text{O-U2-O}$ [deg]	$\angle\text{N-U-N}$ [deg]
4	176.16(11)		62.83(10)
5	176.84(17)		61.59(14)
6	174.48(15)		62.66(12)
7	177.5(2)	177.7(2)	62.08(19), 61.65(19)
8	173.55(18)	175.30(19)	61.57(15)
9	175.80(9)		63.57(7)

X. Bond Valence Summations**Table S15** Bond Valence Summations for hydroxide oxygen atom in complex 4.

O5	Distance (Å)	Bond Valence Sum
Bound atoms		
U1	2.289	0.6249
U1'	2.362	0.5429
	Sum	1.168

Table S16 Bond Valence Summations for hydroxide oxygen atom in complex 6.

O5	Distance (Å)	Bond Valence Sum
Bound atoms		
U1	2.290	0.6237
U1'	2.361	0.5440
	Sum	1.168

Table S17 Bond Valence Summations for oxygen atoms in complex 8.

O7	Distance (Å)	Bond Valence Sum	O8	Distance (Å)	Bond Valence Sum
Bound atoms			Bound atoms		
U1	2.298	0.6142	U1	2.240	0.6868
U2	2.387	0.5173	U2	2.317	0.5921
	Sum	1.132	U2'	2.249	0.6750
				Sum	1.954
OW1					
Bound atoms					
U2	2.541	0.3845			
	Sum	0.3845			

Bond valence summations for selected oxygen atom in **4**, **6**, and **8**. The values indicate that selected oxygen atoms in **4** and **6** are hydroxyl groups, whereas for **8**, values reveal that O7 is a hydroxyl group while O8 is an oxide group.³⁻⁴

XI. References

1. Carter, K. P.; Cahill, C. L., Combining coordination and supramolecular chemistry to explore uranyl assembly in the solid state. *Inorganic Chemistry Frontiers* **2015**, 2 (2), 141-156.
2. Wellington, J. P. W.; Kerridge, A.; Kaltsoyannis, N., Should environmental effects be included when performing QTAIM calculations on actinide systems? A comparison of QTAIM metrics for Cs₂UO₂Cl₄, U(Se₂PPh₂)₄ and Np(Se₂PPh₂)₄ in gas phase, COSMO and PEECM. *Polyhedron* **2016**, 116, 57-63.
3. Brese, N. E.; O'Keeffe, M., Bond-valence parameters for solids. *Acta Crystallographica Section B* **1991**, 47 (2), 192-197.
4. Burns, P. C.; Ewing, R. C.; Hawthorne, F. C., The crystal chemistry of hexavalent uranium; polyhedron geometries, bond-valence parameters, and polymerization of polyhedra. *The Canadian Mineralogist* **1997**, 35 (6), 1551-1570.